

Meson-meson scattering within one loop Chiral Perturbation Theory and its unitarization.

A. Gómez Nicola and J. R. Peláez

Departamento de Física Teórica II, Universidad Complutense de Madrid, 28040– Madrid, Spain
(September, 2001)

We present the complete one-loop calculation of all the two meson scattering amplitudes within the framework of $SU(3)$ Chiral Perturbation Theory, which includes pions, kaons and the eta. In addition, we have unitarized these amplitudes with the coupled channel Inverse Amplitude Method, which ensures simultaneously the good low energy properties of Chiral Perturbation Theory and unitarity. We show how this method provides a remarkable description of meson-meson scattering data up to 1.2 GeV including the scattering lengths and the generation of seven light resonances, which is consistent with previous determination of the chiral parameters. Particular attention is paid to discuss the differences and similarities of this work with previous analysis in the literature.

PACS numbers: 13.75.Lb, 12.39.Fe, 11.80.Et, 14.40.-n

I. INTRODUCTION

In the last twenty years, Chiral Perturbation Theory (ChPT) [1–3] has emerged as a powerful tool to describe the interactions of the lightest mesons. These particles are considerably lighter than the rest of the hadrons, which is nowadays understood as a consequence of the spontaneous breaking of the $SU(3)_L \times SU(3)_R$ chiral symmetry down to $SU(3)_{L+R}$ that would be present in QCD if the three lightest quarks were massless. In such case, the light mesons would correspond to the massless Goldstone bosons associated to the spontaneous chiral symmetry breaking. Of course, quarks are not massless, but their masses are so small compared to the typical hadronic scales, $O(1 \text{ GeV})$, that their explicit symmetry breaking effect also translates into a small mass for the lightest mesons, which become pseudo-Goldstone bosons. Hence, the three pions correspond to the pseudo-Goldstone bosons of the $SU(2)$ spontaneous breaking that would occur if only the u and d quarks were massless, which is a remarkably good approximation. Similarly, the meson octet formed by the pions, the kaons and the eta can be identified with the eight pseudo-Goldstone bosons associated to the $SU(3)$ breaking, when the s quark is also included.

The low energy interactions of pions, kaons and the eta can be described in terms of an effective Lagrangian that follows the $SU(3)_L \times SU(3)_R \rightarrow SU(3)_{L+R}$ spontaneous symmetry breaking pattern. If we do not include any additional field apart from the pseudo-Goldstone bosons, this description will only be valid for energies much below the scale where new states appear. That is, the effective ChPT Lagrangian provides just a low energy description. As a consequence we can organize all the possible terms that respect the symmetry requirements in a derivative (and mass) expansion. Therefore, any amplitude is obtained as a perturbative expansion in powers of the external momenta and the quark masses. The

importance of this formalism is that the theory is renormalizable and predictive, in the following sense: all loop divergences appearing at a given order in the expansion can be absorbed by a finite number of counterterms, or low energy constants, that appear in the Lagrangian at that very same order. Thus, order by order, the theory is finite and depends on a few parameters that can be determined experimentally. Once these parameters are known, any other calculation at that order becomes a prediction. Basically, these are the main ideas underlying ChPT, which has proven very successful to describe the low energy hadron phenomenology (for reviews see [4]).

Despite the success of this approach, it is unfortunately limited to low energies (usually, less than 500 MeV). That is the reason why, over the last few years, there has been a growing interest in extending the applicability range of the chiral expansion to higher energies. Of course, this requires the use of non-perturbative methods to improve the high energy behavior of ChPT amplitudes. These methods include the explicit introduction of heavier resonant states in the Lagrangian [5], resummation of diagrams in a Lippmann-Schwinger or Bethe-Salpeter approach [6], or other methods that unitarize the amplitudes like the Inverse Amplitude Method (IAM) [7,8]. The latter has been generalized to allow for a coupled channel formalism [9], yielding a successful description of the meson-meson scattering amplitudes up to 1.2 GeV, and even generating dynamically seven light resonances.

In principle, these methods recover at low energies the good properties of ChPT, since they use part of the perturbative information. However, it should be noted that, so far, the full results to one loop for all the meson-meson scattering processes were not available in the literature. At present only the $\pi\pi \rightarrow \pi\pi$ [10], $K\pi \rightarrow K\pi$ [10], $\eta\pi \rightarrow \eta\pi$ [10] and the two independent $K^+K^- \rightarrow K^+K^-$, $K^+K^- \rightarrow K^0\bar{K}^0$ [11] amplitudes have been obtained in the $SU(3)$ ChPT framework, although with different procedures and notations. As a

consequence, the IAM has only been applied rigorously to the $\pi\pi$, $K\bar{K}$ final states, whereas for a complete treatment of the whole low energy meson-meson scattering additional approximations had to be done [9]. In particular, the lowest order expansion could not be recovered complete up to $O(p^4)$ thus spoiling the scattering lengths and, in addition, it was not possible to compare directly with the low energy parameters of standard ChPT in dimensional regularization and the $\overline{MS} - 1$ scheme.

In this work, we have calculated all the meson-meson scattering amplitudes at one loop in ChPT. There are three amplitudes that have never appeared published in the literature: $K\eta \rightarrow K\eta$, $\eta\eta \rightarrow \eta\eta$ and $K\pi \rightarrow K\eta$. The other five have been recalculated independently and all of them are given together in a unified notation, ensuring exact perturbative unitarity and also correcting previous misprints. Then, we have applied the coupled channel IAM to describe the whole meson-meson scattering below 1.2 GeV, including low energy data like scattering lengths. This new calculation allows for a direct comparison with the standard low energy constants of ChPT and that is why we have made a considerable effort in estimating the uncertainties in all our results. which are in very good agreement with the present determinations obtained from low energy data without unitarization. The main differences of this work with [9] are that we consider the full one-loop results for the amplitudes, ensuring their finiteness and scale independence in dimensional regularization, we take into account the new processes mentioned above and we are able to describe more accurately the low energy region. This had already been achieved for the $\pi\pi$ $K\bar{K}$ system only in [11], but here we complete this task for the whole meson-meson scattering.

The paper is organized as follows. In section II we review the main features concerning the meson-meson scattering calculations at one-loop in ChPT. The final results for the amplitudes have been collected in Appendix B due to their length. The definition of partial waves and unitarity is discussed in section III, and the IAM is presented in section IV. In section V, we review the available data on meson-meson scattering. In sections VI and VII we first use the IAM with present determinations of the low energy constants and next we make a fit to the data commented in section V. Our conclusions are summarized in section VIII. Apart from the amplitudes in Appendix B, we have also collected some useful formulae in Appendix A.

II. MESON MESON SCATTERING AT ONE LOOP

The lowest order Lagrangian for SU(3) Chiral Perturbation Theory is:

$$\mathcal{L}_2 = \frac{f_0^2}{4} \langle \partial_\mu U^\dagger \partial^\mu U + M_0(U + U^\dagger) \rangle, \quad (1)$$

where f_0 is the pion decay constant in the SU(3) chiral limit and the angular brackets stand for the trace of the 3×3 matrices. The matrix U collects the pseudo-Goldstone boson fields π, K, η through $U(\Phi) = \exp(i\sqrt{2}\Phi/f_0)$, where

$$\Phi(x) \equiv \begin{pmatrix} \frac{1}{\sqrt{2}}\pi^0 + \frac{1}{\sqrt{6}}\eta & \pi^+ & K^+ \\ \pi^- & -\frac{1}{\sqrt{2}}\pi^0 + \frac{1}{\sqrt{6}}\eta & K^0 \\ K^- & \bar{K}^0 & -\frac{2}{\sqrt{6}}\eta \end{pmatrix}. \quad (2)$$

and M_0 is the tree level mass matrix. Throughout this paper we will be assuming the isospin limit, so that M_0 is given by

$$M_0 = \begin{pmatrix} M_{0\pi}^2 & 0 & 0 \\ 0 & M_{0\pi}^2 & 0 \\ 0 & 0 & 2M_{0K}^2 - M_{0\pi}^2 \end{pmatrix}. \quad (3)$$

As a matter of fact, from these definitions, it can be easily seen that the tree level masses satisfy the Gell-Mann–Okubo relation [13]: $4M_{0K}^2 - M_{0\pi}^2 - 3M_{0\eta}^2 = 0$, that will be very useful for simplifying the amplitudes.

From the Lagrangian in Eq.(1), one can obtain the $O(p^2)$ amplitudes just by calculating the corresponding tree level Feynman diagrams. In order to obtain the $O(p^4)$ contributions, one has to consider loop diagrams, whose generic topology is given in Fig.1, which will generate UV divergences. If loop integrals are regularized with dimensional regularization, which preserves the chiral symmetry constraints, the divergences can be reabsorbed in the chiral parameters L_i of the fourth order Lagrangian:

$$\begin{aligned} \mathcal{L}_4 = & L_1 \langle \partial_\mu U^\dagger \partial^\mu U \rangle^2 + L_2 \langle \partial_\mu U^\dagger \partial_\nu U \rangle \langle \partial^\mu U^\dagger \partial^\nu U \rangle \\ & + L_3 \langle \partial_\mu U^\dagger \partial^\mu U \partial_\nu U^\dagger \partial^\nu U \rangle + L_4 \langle \partial_\mu U^\dagger \partial^\mu U \rangle \langle U^\dagger M_0 + M_0^\dagger U \rangle \\ & + L_5 \langle \partial_\mu U^\dagger \partial^\mu U (U^\dagger M_0 + M_0^\dagger U) \rangle + L_6 \langle U^\dagger M_0 + M_0^\dagger U \rangle^2 \\ & + L_7 \langle U^\dagger M_0 - M_0^\dagger U \rangle^2 + L_8 \langle M_0^\dagger U M_0^\dagger U + U^\dagger M_0 U^\dagger M_0 \rangle, \end{aligned} \quad (4)$$

where the terms which couple to external sources, like gauge fields, are omitted [2,3]. The L_i constants are related with the renormalized $L_i^r(\mu)$ generically as $L_i = L_i^r(\mu) + \Gamma_i \lambda$ [3] where μ is the renormalization scale,

$$\lambda = \frac{\mu^{d-4}}{16\pi^2} \left[\frac{1}{d-4} - \frac{1}{2} (\log 4\pi - \gamma + 1) \right], \quad (5)$$

γ is the Euler constant and the Γ_i coefficients can be found in [3]. We remark that the L_3 and L_7 constants are not renormalized and are therefore scale independent, i.e., $\Gamma_3 = \Gamma_7 = 0$.

Thus, up to fourth order one has to consider the tree level diagrams from $O(p^2)$ and $O(p^4)$, together with the one-loop diagrams in Fig.1. We stress that mass and wave function renormalizations should be accounted for to the same order. The latter are schematically represented by the tadpole diagram (e) in Fig.1. As customary, we define the bare fields in terms of the renormalized

ones as $\pi = Z_\pi^{1/2} \pi^{ren}$ and so on for the kaons and eta, so that scalar fields have finite canonical kinetic terms. Taking into account all the different contributions from diagrams of type (e) in Fig.1 plus those tree level diagrams coming from \mathcal{L}_4 , one obtains:

$$\begin{aligned}
Z_\pi &= 1 + \frac{4}{3}\mu_\pi + \frac{2}{3}\mu_K - \frac{4\lambda}{3f_0^2} (2M_{0\pi}^2 + M_{0K}^2) \\
&\quad - \frac{8}{f_0^2} [2L_4^r M_{0K}^2 + (L_4^r + L_5^r) M_{0\pi}^2], \\
Z_K &= 1 + \frac{1}{2}\mu_\pi + \mu_K + \frac{1}{2}\mu_\eta - \frac{2\lambda}{3f_0^2} (M_{0\pi}^2 + 5M_{0K}^2) \\
&\quad - \frac{8}{f_0^2} [(2L_4^r + L_5^r) M_{0K}^2 + L_4^r M_{0\pi}^2], \\
Z_\eta &= 1 + 2\mu_K - \frac{4\lambda}{f_0^2} M_{0K}^2 \\
&\quad - \frac{8}{3f_0^2} [(3L_4^r - L_5^r) M_{0\pi}^2 + 2(3L_4^r + 2L_5^r) M_{0K}^2], \quad (6)
\end{aligned}$$

where

$$\mu_i = \frac{M_i^2}{32\pi^2 f_0^2} \log \frac{M_i^2}{\mu^2}, \quad (7)$$

with $i = \pi, K, \eta$.

Note that the wave function renormalization constants Z_i contain a divergent part and they are scale dependent.

As for the mass renormalizations, the physical pion and kaon masses are given in terms of the tree level ones as [3]:

$$\begin{aligned}
M_\pi^2 &= M_{0\pi}^2 \left[1 + \mu_\pi - \frac{\mu_\eta}{3} + \frac{16M_{0K}^2}{f_0^2} (2L_6^r - L_4^r) \right. \\
&\quad \left. + \frac{8M_{0\pi}^2}{f_0^2} (2L_6^r + 2L_8^r - L_4^r - L_5^r) \right], \\
M_K^2 &= M_{0K}^2 \left[1 + \frac{2\mu_\eta}{3} + \frac{8M_{0\pi}^2}{f_0^2} (2L_6^r - L_4^r) \right. \\
&\quad \left. + \frac{8M_{0K}^2}{f_0^2} (4L_6^r + 2L_8^r - 2L_4^r - L_5^r) \right], \\
M_\eta^2 &= M_{0\eta}^2 \left[1 + 2\mu_K - \frac{4}{3}\mu_\eta + \frac{8M_{0\eta}^2}{f_0^2} (2L_8^r - L_5^r) \right. \\
&\quad \left. + \frac{8}{f_0^2} (2M_{0K}^2 + M_{0\pi}^2) (2L_6^r - L_4^r) \right] \\
&\quad + M_{0\pi}^2 \left[-\mu_\pi + \frac{2}{3}\mu_K + \frac{1}{3}\mu_\eta \right] \\
&\quad + \frac{128}{9f_0^2} (M_{0K}^2 - M_{0\pi}^2)^2 (3L_7^r + L_8^r) \quad (8)
\end{aligned}$$

According to the chiral power counting, we have to use Eq.(6) and Eq.(8) only in the tree level part of the amplitudes. In fact, the mass renormalization Eq.(8) affects only the mass terms coming from the Lagrangian in Eq.(1) and not the masses coming from the kinematics of the corresponding process. As it will be seen below,

we will not need the mass renormalization of M_η in any of our expressions.

The meson decay constants are also modified to one loop. It will be convenient for our purposes to write all the one-loop amplitudes in terms of a single decay constant, which we have chosen to be f_π . For that reason and for an easier comparison with previous results in the literature, we also give here the result for the meson decay constants to one loop [3]:

$$\begin{aligned}
f_\pi &= f_0 \left[1 - 2\mu_\pi - \mu_K + \frac{4M_{0\pi}^2}{f_0^2} (L_4^r + L_5^r) + \frac{8M_{0K}^2}{f_0^2} L_4^r \right], \\
f_K &= f_0 \left[1 - \frac{3\mu_\pi}{4} - \frac{3\mu_K}{2} - \frac{3\mu_\eta}{4} + \frac{4M_{0\pi}^2}{f_0^2} L_4^r \right. \\
&\quad \left. + \frac{4M_{0K}^2}{f_0^2} (2L_4^r + L_5^r) \right], \\
f_\eta &= f_0 \left[1 - 3\mu_K + \frac{4L_4^r}{f_0^2} (M_{0\pi}^2 + 2M_{0K}^2) + \frac{4M_{0\eta}^2}{f_0^2} L_5^r \right]. \quad (9)
\end{aligned}$$

It is important to stress that both the physical masses in Eq.(8) and the decay constants in Eq.(9) are finite and scale independent.

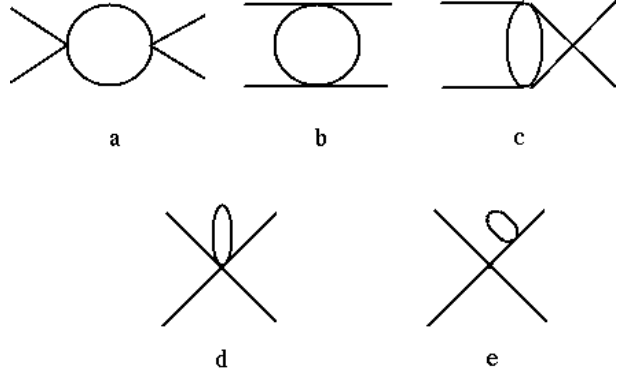


FIG. 1. Generic One-loop Feynman diagrams that have to be evaluated in meson-meson scattering.

Therefore, the one-loop ChPT scattering amplitude (renormalized and scale independent) for a given process will have the generic form:

$$T(s, t, u) = T_2(s, t, u) + T_4^{pol}(s, t, u) + T_4^{uni}(s, t, u) \quad (10)$$

where s, t, u are the Mandelstam variables. Here, T_2 is the tree level contribution from the Lagrangian in Eq.(1), whereas T_4^{pol} contains the fourth-order terms which are polynomials in s, t, u . Those polynomials have four possible origins: tree level terms from the Lagrangian in Eq.(4) proportional to L_i^r , other polynomial terms proportional to L_i with $i = 4 \dots 8$ coming from the mass and decay constant renormalization in eqs.(8) and (9), terms proportional to μ_i coming from tadpole diagrams ((d) and (e) in Figure 1) and finally pure polynomial fourth-order terms which stem from our parametrization of the

one-loop functions (see Appendix A). Let us remark that, for technical reasons explained in section III.B, we have chosen to write all our amplitudes in terms of f_π only since, using eqs.(fpis), f_K and f_η can be expressed in terms of f_π , L_4^r and L_5^r . In addition, T_4^{uni} stands for the contribution of diagrams (a),(b) and (c) in Figure 1. These contributions not only contain the imaginary parts required by unitarity but also yield the correct analytic structure for the perturbative amplitudes, as it will be discussed below. We remark that all the terms in T_4^{uni} will be proportional to the \bar{J} and \bar{J} functions defined in Appendix A.

Using crossing symmetry it is not difficult to see that there are only eight independent meson-meson amplitudes. We have calculated these amplitudes to one loop in $SU(3)$ ChPT. They are given in Appendix B. Three of these amplitudes had not been calculated before, namely $\bar{K}^0\eta \rightarrow \bar{K}^0\eta$, $\eta\eta \rightarrow \eta\eta$ and $K\eta \rightarrow K\pi^0$. For the rest, we have checked that our amplitudes coincide with previous results [10,11] up to differences in notation and different simplification schemes, equivalent up to $O(p^6)$. In particular, since we are interested in the “exact” form of perturbative unitarity (see below), we have written our final results in terms of a single pion decay constant, f_π , and we have used the Gell-Mann–Okubo relation taking care of preserving exact perturbative unitarity. Furthermore, we have explicitly checked that all the amplitudes remain finite and scale independent.

Finally, we wish to add a remark about $\eta - \eta'$ mixing, since the physical η is indeed a mixture of the $U(3)$ octet and singlet pseudoscalars, whereas in this work we are only using the standard $SU(3)$ ChPT. One may wonder then if our description of the η is just that of the pseudoscalar octet component, since in this Lagrangian the singlet field is not an explicit degree of freedom. However, it has been shown [12] that the standard framework results from an expansion in powers of the inverse powers of the “topological susceptibility” of the complete $U(3)$ Lagrangian. In that context the η' is considered as a massive state (that is why it does not count as an explicit degree of freedom) but the singlet component generates a correction to L_7 . Note that, indeed, the mass of the η contains an L_7 contribution, and that is why we can use M_η in eq.(8) with its physical value, whereas the $M_{0\eta}$ is the one satisfying the Gell-Mann–Okubo relation exactly. Therefore, our approach can be understood as the lowest order approximation to the $\eta - \eta'$ mixing problem, where all the effects of the mixing appear only through L_7 . Since we will only compare with data in states with one η at most, and below 1200 MeV, our results seem to suggest that this approximation, although somewhat crude, is enough with the present status of the experimental data. Indeed, we will see that the values that we obtain for L_7 are in perfect agreement with those given in the literature (and this comparison can now be done because we have the complete one loop amplitudes renormalized in the standard way).

III. PARTIAL WAVES AND UNITARITY

A. Partial waves

Let us denote by $T_{ab}^{IJ}(s)$ the partial wave for the process $a \rightarrow b$, i.e, the projection of the amplitude for that process with given total isospin I and angular momentum J . That is, if $T_{ab}^I(s, t, u)$ is the isospin combination with total isospin I , one has

$$T_{ab}^{IJ}(s) = \frac{1}{32N\pi} \int_{-1}^1 dx P_J(x) T_{ab}^I(s, t(s, x), u(s, x)) \quad (11)$$

where $t(s, x), u(s, x)$ are given by the kinematics of the process $a \rightarrow b$ with $x = \cos \theta$, the scattering angle in the center of mass frame.

Note that we are normalizing the partial waves including a factor N , such that $N = 2$ if all the particles in the process are identical and $N = 1$ otherwise. Recall that, since we are working in the isospin limit, the three pions are considered as identical, so that $N = 2$ only for the $\pi\pi \rightarrow \pi\pi$ and $\eta\eta \rightarrow \eta\eta$ processes.

We shall comment now on the T_{ab}^I amplitudes for every possible process involving π, K, η . Using crossing symmetry and assuming isospin symmetry exactly, we will determine the number of independent amplitudes for each process. The discussion is general and there is no need to invoke ChPT, although we will refer to the results for the amplitudes in Appendix B, which are the one-loop ChPT results.

- $\pi\pi \rightarrow \pi\pi$ scattering: There is only one independent amplitude, so that one has

$$\begin{aligned} T^0(s, t, u) &= 3T(s, t, u) + T(t, s, u) + T(u, t, s), \\ T^1(s, t, u) &= T(t, s, u) - T(u, t, s), \\ T^2(s, t, u) &= T(t, s, u) + T(u, t, s), \end{aligned}$$

where $T(s, t, u)$ is the $\pi^+\pi^- \rightarrow \pi^0\pi^0$ amplitude. At one-loop in ChPT it is given in Appendix B, Eq.(B4).

- $K\pi \rightarrow K\pi$ scattering: Crossing symmetry allows us to write the $I = 1/2$ in terms of the $I = 3/2$ one as

$$T^{1/2}(s, t, u) = \frac{1}{2} \left[3T^{3/2}(u, t, s) - T^{3/2}(s, t, u) \right]. \quad (12)$$

Here, $T^{3/2}(s, t, u)$ is the $K^+\pi^+ \rightarrow K^+\pi^+$ amplitude, whose expression at one-loop within ChPT corresponds to Eq.(B5).

- $K\bar{K} \rightarrow K\bar{K}$ scattering: We can write the isospin amplitudes as

$$\begin{aligned}
T^0(s, t, u) &= T_{ch}(s, t, u) + T_{neu}(s, t, u), \\
T^1(s, t, u) &= T_{ch}(s, t, u) - T_{neu}(s, t, u),
\end{aligned} \tag{13}$$

where T_{ch} and T_{neu} are, respectively, the amplitudes for the processes $K^+K^- \rightarrow K^+K^-$ and $\bar{K}^0K^0 \rightarrow K^+K^-$. Their expressions to one loop correspond to Eqs.(B7) and (B8), respectively.

- $K\bar{K} \rightarrow \pi\pi$ scattering: In this case, one has

$$\begin{aligned}
T^0(s, t, u) &= \frac{\sqrt{3}}{2} \left[T^{3/2}(u, s, t) + T^{3/2}(t, s, u) \right], \\
T^1(s, t, u) &= \frac{1}{\sqrt{2}} \left[T^{3/2}(u, s, t) - T^{3/2}(t, s, u) \right],
\end{aligned} \tag{14}$$

where $T^{3/2}(s, t, u)$ is the $K^+\pi^+ \rightarrow K^+\pi^+$ amplitude, given in Appendix B for one-loop ChPT, Eq.(B5).

- $K\eta \rightarrow K\eta$ scattering: This is a pure $I = 1/2$ process. The one-loop amplitude can be read directly from Eq.(B2)
- $\bar{K}K \rightarrow \eta\eta$ scattering: This is an $I = 0$ process that using crossing symmetry can be obtained from the previous amplitude as follows:

$$T_{\bar{K}^0K^0 \rightarrow \eta\eta}(s, t, u) = T_{\bar{K}^0\eta \rightarrow \bar{K}^0\eta}(t, s, u). \tag{15}$$

- $K\eta \rightarrow K\pi$ scattering: This is also an $I = 1/2$ process, whose amplitude correctly normalized, is

$$T^{1/2}(s, t, u) = -\sqrt{3} T_{\bar{K}^0\eta \rightarrow \bar{K}^0\pi^0}(s, t, u), \tag{16}$$

where the one-loop expression for $\bar{K}^0\eta \rightarrow \bar{K}^0\pi^0$ can be found in Eq.(B3)

- $\bar{K}K \rightarrow \pi\eta$ scattering: This is a $I = 1$ process related to the $\bar{K}^0\eta \rightarrow \bar{K}^0\pi^0$ amplitude by crossing symmetry, i.e:

$$T^1(s, t, u) = -\sqrt{2} T_{\bar{K}^0\eta \rightarrow \bar{K}^0\pi^0}(t, s, u). \tag{17}$$

- $\pi\eta \rightarrow \pi\eta$ scattering: This is a pure $I = 1$ isospin amplitude whose one-loop ChPT expression can be read directly from Eq.(B6).
- $\pi\pi \rightarrow \eta\eta$ scattering: Now $I = 0$ and the amplitude is obtained from the previous one by crossing, as

$$T_{\pi^0\pi^0 \rightarrow \eta\eta}(s, t, u) = T_{\pi^0\eta \rightarrow \pi^0\eta}(t, s, u). \tag{18}$$

- $\eta\eta \rightarrow \eta\eta$ scattering: Here, $I = 0$ and the corresponding one-loop amplitude can also be read directly from Eq.(B1).

In this paper we will be interested in the case when there are several coupled states for a given choice of I, J , i.e: the coupled channel case. In particular, with the above normalization, the relationship between the T -matrix elements T_{ab}^{IJ} and the S -matrix ones is given for two coupled channels ($a, b = 1, 2$) by

$$S_{11} = 1 + 2i \sigma_1 T_{11}, \tag{19}$$

$$S_{22} = 1 + 2i \sigma_2 T_{22}, \tag{20}$$

$$S_{12} = S_{21} = 2i \sqrt{\sigma_1 \sigma_2} T_{12}, \tag{21}$$

where the IJ superscripts have been suppressed to ease the notation and we have used that due to time reversal invariance, $T_{ij} = T_{ji}$. Here, $\sigma_i = 2q_i/\sqrt{s}$ where q_i is the center of mass momentum in the state i . Note that σ_i is nothing but the phase space of that state at \sqrt{s} . In the $I = 0$ channel above the $\eta\eta$ threshold we will use the corresponding generalization in the case of three channels.

B. Unitarity

The S matrix should be unitary, i.e, $SS^\dagger = 1$. In case there is only one state available, that means that S can be parametrized in terms of a single observable, which is customarily chosen as the phase shift. For the case of two channels, the elements S_{ij} are organized in a unitary 2×2 matrix, containing only three independent parameters. We will follow the standard parametrization:

$$S = \begin{pmatrix} \eta e^{2i\delta_1} & i\sqrt{1-\eta^2} e^{i(\delta_1+\delta_2)} \\ i\sqrt{1-\eta^2} e^{i(\delta_1+\delta_2)} & \eta e^{2i\delta_2} \end{pmatrix}. \tag{22}$$

where the δ_i are the phase shifts and η is the inelasticity.

The unitarity relation translates into relations for the elements of the T matrix of a particularly simple form for the partial waves. For instance, if there is only one possible state, "1", for a given choice of I, J , the partial wave T_{11} satisfies Eq.(19), so that unitarity means

$$\text{Im} T_{11} = \sigma_1 |T_{11}|^2 \Rightarrow \text{Im} T_{11}^{-1} = -\sigma_1, \tag{23}$$

In principle, the above equation *only holds above threshold* up to the energy where another state, "2", is physically accessible. If there are two states available, then the T matrix elements satisfy

$$\text{Im} T_{11} = \sigma_1(s) |T_{11}|^2 + \sigma_2 |T_{12}|^2,$$

$$\text{Im} T_{12} = \sigma_1 T_{11} T_{12}^* + \sigma_2 T_{12} T_{22}^*,$$

$$\text{Im} T_{22} = \sigma_1 |T_{12}|^2 + \sigma_2 |T_{22}|^2.$$

In matrix form they read,

$$\text{Im} T = T \Sigma T^* \Rightarrow \text{Im} T^{-1} = -\Sigma, \tag{24}$$

with

$$T = \begin{pmatrix} T_{11} & T_{12} \\ T_{12} & T_{22} \end{pmatrix}, \quad \Sigma = \begin{pmatrix} \sigma_1 & 0 \\ 0 & \sigma_2 \end{pmatrix}, \quad (25)$$

which allows for an straightforward generalization to the case of n accessible states by using $n \times n$ matrices.

One must bear in mind that the unitarity relations imply that the partial waves are bounded as the energy increases. For instance, in the one channel case, from Eq.(23) we can write:

$$T_{11} = \frac{\sin \delta}{\sigma_1} e^{i\delta} \quad (26)$$

where δ is the phase of t_{11} .

Note that all the unitarity relations, Eqs.(23) and (24), are linear on the left hand side and quadratic on the right. As a consequence, if one calculates the amplitudes perturbatively as truncated series in powers of an expansion parameter, say $T = T_2 + T_4 + \dots$, the unitarity equations will never be satisfied exactly. In particular, for ChPT that means that unitarity can only be satisfied *perturbatively*, i.e.:

$$\begin{aligned} \text{Im } T_2 &= 0, \\ \text{Im } T_4 &= T_2 \Sigma T_2, \\ &\dots \end{aligned} \quad (27)$$

where the latter is only satisfied *exactly* if one is careful to express T_4 in terms of masses and decay constants consistently with the choice made for T_2 . That has not always been the case in the literature and that is one of the reasons why we have recalculated some processes: all our results satisfy exact perturbative unitarity. Otherwise there are additional $O(p^6)$ terms in Eq.(27). As we will see below, this will be relevant to obtain a simple formula for the unitarized amplitudes. Our choice has been to rewrite all the f_K and f_η contained in the amplitudes in terms of f_π , L_4^r and L_5^r using the relations in eq.(9).

The deviations from Eq.(24) are more severe at high energies, and in particular in the resonance region, since unitarity implies that the partial waves are bounded, see Eq.(26), which cannot be satisfied by a polynomial. Generically, in the resonance region, the unitarity bounds are saturated. If a polynomial is adjusted to saturate unitarity in a given region, in general, it will break the unitarity bound right afterward. Another way of putting it is that resonances are associated to poles in the complex plane, that will never be reproduced with polynomials.

For all these reasons, if we are interested in extending the good properties of ChPT to higher energies, we have to modify the amplitudes, imposing unitarity and a functional form that allows for poles in the complex plane. This will be achieved with the Inverse Amplitude Method.

IV. THE COUPLED CHANNEL INVERSE AMPLITUDE METHOD

As it can be seen from the unitarity condition in Eq.(24), the imaginary part of the Inverse Amplitude is known exactly above the corresponding thresholds, namely, $\text{Im } T^{-1} = -\Sigma$. Indeed, any amplitude satisfying the unitarity constraint should have the following form:

$$T = (\text{Re } T^{-1} - i\Sigma)^{-1}. \quad (28)$$

Consequently, we should only have to calculate the real part of T^{-1} . As a matter of fact, many unitarization methods are just different approximations to $\text{Re } T^{-1}$ (see [9] for details). The idea behind the Inverse Amplitude Method (IAM) is to use the formula right above, but approximating $\text{Re } T^{-1}$ with ChPT. Since we have $T \simeq T_2 + T_4 + \dots$. Then

$$T^{-1} \simeq T_2^{-1}(1 - T_4 T_2^{-1} + \dots), \quad (29)$$

$$\text{Re } T^{-1} \simeq T_2^{-1}(1 - (\text{Re } T_4) T_2^{-1} + \dots), \quad (30)$$

so that multiplying Eq.(28) by $T_2 T_2^{-1}$ on the left and $T_2^{-1} T_2$ on the right, we find

$$T \simeq T_2(T_2 - \text{Re } T_4 - i T_2 \Sigma T_2)^{-1} T_2. \quad (31)$$

At this point, if the amplitude satisfy “exact perturbative unitarity”, namely Eq.(27), we can simplify the above equation to obtain a simple expression

$$T \simeq T_2(T_2 - T_4)^{-1} T_2, \quad (32)$$

This is the generalization of the IAM to coupled channels. Note that this formula only ensures exact unitarity if T_4 satisfies “exact perturbative unitarity”.

The IAM was first applied to just one elastic channel [7] and it was able to reproduce well the $\pi\pi$ and πK scattering phase shifts below the $K\bar{K}$ and $K\eta$ thresholds, respectively. In addition it was able to generate the σ (now called $f_0(400 - 1200)$) the ρ and the K^* resonances [8]. Furthermore, it was shown how the formula for the one channel IAM can be justified in terms of dispersion relations [8], which allowed for the analytic continuation to the complex plane and the identification of the pole associated to each resonance in the second Riemann sheet.

In view of Eq.(32), it may seem necessary to know the complete $O(p^4)$ ChPT calculation of each one of the T matrix elements. Nevertheless, one could use a further approximation and calculate only the s-channel loops (Fig.1a), which are the only responsible for the unitarity cut and are supposed to dominate in the resonant region. This was the approach followed in [9], having in mind that the complete ChPT calculations were not available at that time for any meson-meson scattering two-channel matrix. The results were remarkable, reproducing up to 1.2 GeV seven (I, J) meson-meson scattering channels (17 amplitudes), and even generating seven resonances. However, the fact that the s-channel loops

were regularized with a cutoff, together with the omission of crossed loops and tadpoles, made impossible to compare the chiral parameters with those of standard ChPT (still, they had the correct order of magnitude, as expected). Besides, the low energy ChPT predictions were recovered only partially. This motivated the authors in [11] to calculate the full $O(p^4)$ $K^+K^- \rightarrow K^+K^-$ and $K^+K^- \rightarrow K^0\bar{K}^0$ amplitudes*, which allowed for the unitarization with Eq.(32) of the $(I, J)=(0, 0)$ and $(1, 1)$ channels. This approach yielded again a good high energy description but also reproduced simultaneously the low energy $\pi\pi$ scattering lengths. All these results were obtained with L_i parameters compatible with those of standard ChPT [11].

As we have seen in the previous section, we have calculated the last three independent $O(p^4)$ meson-meson scattering amplitudes that were still missing. They are given in Appendix B in an unified notation with the other five that we have recalculated independently (correcting some minor misprints in the literature). Therefore, we are now ready to unitarize the complete meson-meson scattering by means of Eq.(32).

However, at this point we have to recall that for a given energy, Eq.(32) has only been justified for a matrix whose dimension is exactly the number of states accessible at that energy. The reason is that the unitarity relation, Eq.(24), increases its dimensionality each time we cross a new threshold. Thus, for instance, in $\pi\pi$ scattering, one should use the one dimensional IAM up to the $K\bar{K}$ threshold, then the two dimensional IAM, etc....although this procedure yields discontinuities on each threshold, instead of a single analytic function. Another possibility [9] is to use the IAM with the highest possible dimensionality of the I, J channel for all energies[†]. This second possibility yields an analytic (and hence continuous) function, but it may not satisfy unitarity exactly at all energies, namely, when the number of opened channels is smaller than the dimensionality of the IAM formula. Following with the $\pi\pi - K\bar{K}$ example, if we use the 2-dimensional IAM formula, we will have exact unitarity ensured above the $K\bar{K}$ threshold, but not below. In particular, if we still use the 2-dimensional IAM be-

low $K\bar{K}$ threshold, the IAM $\pi\pi$ scattering element will have an additional spurious contribution from the imaginary part of the $K\bar{K}$ scattering left cut, which extends up to $\sqrt{s} = 4(M_K^2 - M_\pi^2)$. This is a well known and lasting problem in the literature [14–16] that affects also other unitarization methods, like the K-matrix [15]. As a matter of fact, several years ago [14] it was suggested that the physical solution would probably be an interpolation between the two just mentioned approaches. However, in the context of ChPT and the IAM, and for the $\pi\pi - K\bar{K}$ channels, it was found [11] that the violations of unitarity are, generically, of the order of a few percent only. We have confirmed this result but now for the whole meson-meson scattering sector. Even the threshold parameters can be accurately reproduced, since they are defined through the real part of the amplitudes which are almost not affected by the spurious part. The origin of this problem is that the IAM in Eq.(32) mixes the left cuts of all the channels involved when performing the inverse of the $T_2 - T_4$ matrix. Thus, it is not able to reproduce the left-cut singularities correctly [8,17], although numerically their contribution is negligible when all the observables are expressed in terms of real parts of the amplitude, and *taking into account the present status of the data and the uncertainties in the L_i* .

In this paper we have chosen to show the second approach, since the one-dimensional IAM has been thoroughly studied in [8]. Very recently there have been proposed dispersive approaches [16] to circumvent this problem in the $\pi\pi - K\bar{K}$ system, but they involve the calculation of left-cut integrals that are hard to estimate theoretically. It would be interesting to have them extended and related to the ChPT formalism, but that is beyond the scope of this work. The fact that we use the higher dimensional IAM formalism, which contains spurious cuts, does not allow for a clean continuation to the complex plane. Nevertheless, since poles associated to resonances have already been found in the one-dimensional case [8] and in other approximated coupled channel IAM approaches [9], we leave their description for a generalized IAM approach with better analytic properties [18]. In this work we will concentrate on physical s values, and the compatibility of the unitarized description of resonances and low energy data with existing determinations of the chiral parameters. Nevertheless we will also show that this can also be achieved with the first, discontinuous, approach.

V. MESON-MESON SCATTERING DATA

Let us then comment on the data available for each channel:

Channel $(I, J)=(1, 1)$ For the energies considered here, the two states that may appear in this channel are $\pi\pi$ and $K\bar{K}$. In Figs.2a and 3a, we plot the data on the $\pi\pi$ scattering phase shift obtained from [19] and

*An erratum for these amplitudes has appeared published when preparing this work. The previous results and conclusions in [11] are nevertheless correct, since the errata did not affect the numerical calculations. We thank J.A. Oller for discussions and for letting us check that their corrected amplitudes coincide with ours.

[†]As a technical remark, let us note that in such case, the IAM has to be rederived in terms of the partial waves T_{ab} divided by the CM momenta of the initial and final states, to ensure that this new amplitudes are real at lowest order. From there the derivation follows the same steps, and we recover the very same Eq.(32) by multiplying by the initial and final state momenta in the end.

[20], which correspond to the squares and triangles respectively. Let us remark that the first set of data points tends to be between two and three standard deviations higher than the second when the phase shift is higher than 90 degrees, and the other way around for smaller values of the phase shift (note that error bars are smaller than the data symbols). Thus the data sets are not quite consistent with one another, which could be fixed with the addition of a systematic error of the order of a few percent.

This channel is completely dominated by the $\pi\pi$ state and there is almost no inelasticity due to $K\bar{K}$ production below 1200 MeV. The $(1 - \eta_{11}^2)/4$ points from the inelasticity analysis given in [21] are shown in the lowest part of Figs.2.d and 3.d.

Channel (I,J)=(0,0) For this channel we may have up to three states, namely $\pi\pi$, $K\bar{K}$ and $\eta\eta$. In this case, there are three observables with several sets of data, which, as can be seen in Figs.2.b,c and d, are somewhat incompatible between themselves when only considering the errors quoted in the experiments. Again, they become compatible if we assume a systematic error of a few percent. For the $\pi\pi$ scattering phase shift (δ_{00} , see Fig.2.b), the experimental data shown come from: different analysis of the CERN-Munich Collaboration [22] (open square), as well as from [19] (solid square), [23] (solid triangle) and [24] (solid circle). Concerning the $\pi\pi \rightarrow K\bar{K}$ phase shift, the data in Figs.2.c and 3.c corresponds to: [21] (solid triangle) and [25] (solid square) and they are reasonably compatible, mainly due to the large errors in the first set. Finally, we are also showing in Figs.2.d and 3.d the data for $(1 - \eta_{00}^2)/4$, since it is customary to represent in that way the values of the inelasticity η_{00} . The experimental results are rather confusing here, mainly up to 1100 MeV, due to problems in the normalization. From the data shown in the figure, we have only fitted to those coming from: [25] (solid square), [26] (solid triangle), [27] (open square) and [28] (open circle). There is a disagreement in the normalization with the data of [29] up to a factor of 2 (see [30] for discussion). We have not included the latter in the fit, mostly because in the analysis of [29] they neglect the unitarity constraint, which in our approach is satisfied exactly at those energies.

Channel (I,J)=(2,0) There is only the $\pi\pi$ state and so we only display in Fig.2.e and 3.e the δ_{20} phase shifts again from the CERN-Munich Collaboration [31] (open square) and the CERN-Saclay Collaboration [32] (solid triangle).

Low energy K_{l4} decay data. This reaction is particularly important since it yields very precise information on the $\delta_{00} - \delta_{11}$ combination of $\pi\pi$ scattering phase shifts at very low energies. In Figs.2.f and 3.f we show the data from the Geneva-Saclay group [33] (solid triangles) and the very recent, and more precise, data from E865 collaboration at Brookhaven [34] (solid squares).

Channel (I,J)=(1/2,1) Here the possible states are $K\pi$ and $K\eta$. We have plotted in Figs 2.g and 3.g data

from the following experiments: [35] (solid square) [36] (solid triangle). Note that the first set is systematically lower than the second, which is newer and more precise. Nevertheless, they are compatible thanks mostly to the large error bars on the first set.

Channel (I,J)=(1/2,0) Here the states are also $K\pi$ and $K\eta$. The data in Figs 2.h and 3.h come from the following experiments: [35] (solid square), [37] (open triangle), [38] (open diamond), [36] (solid triangle), [39] (open square). It can be easily noticed that not all the data sets are compatible within errors, but once again they can be reconciled by assuming a systematic error of the order of a few percent.

Channel (I,J)=(3/2,0) The only state here is πK . In this case we have plotted in Figs.2.i and 3.i, data sets from [36] (solid triangle) and [40] (solid square). The latter is somewhat lower than the former, although they are compatible mostly due to the large errors in [36]

Channel (I,J)=(1,0) The possible states for this case are $\pi\eta$ and $K\bar{K}$. We have plotted in Figs 2.j and 3.j the $\pi\eta$ effective mass distribution from the $pp \rightarrow p(\eta\pi^+\pi^-)p$ reaction studied by the WA76 Collaboration [41]. In order to reproduce this data, we are using

$$\frac{d\sigma_{\pi\eta}}{dE_{cm}} = c p_{\pi\eta} |T_{12}^{10}|^2 + \text{background}. \quad (33)$$

Where the c factor accounts for the normalization of the mass distribution and the dashed curve in those figures corresponds to a background due to other resonances apart from the $a_0(980)$ (see [41] for details).

Once we have described the data on the different channels, we will first compare with the IAM “predictions” from the present values of the ChPT low energy constants, and later we will fit these data by means of the IAM.

VI. THE IAM WITH PRESENT LOW ENERGY CONSTANT DETERMINATIONS

In this section we will comment on the results of applying the coupled channel IAM using the low energy constants from standard ChPT. Since the values of these constants have been determined from low energy data or large N_c arguments, the high energy results could be considered as predictions of the IAM. For our calculations we have used: $f_\pi = 92.4$ MeV, $M_\pi = 139.57$ MeV, $M_K = 495.7$ MeV and $M_\eta = 547.45$ MeV.

In the second column of Table I we list the values obtained from a very recent and precise two-loop $O(p^6)$ analysis of K_{l4} decays [42]. Note that the errors are only statistical. In the next column we list the central values of the same analysis but only at $O(p^4)$. In the fourth column we list the values from another set where L_1, L_2, L_3 are taken from an overall fit to K_{e4} and $\pi\pi$ data [43] and the rest are taken from [2]. Note that all of them

are pretty compatible and, except for L_5 , the size of the error bars is comparable.

	K_{l4} decays $O(p^6)$	K_{l4} decays $O(p^4)$	ChPT
$L_1^r(M_\rho)$	0.53 ± 0.25	0.46	0.4 ± 0.3
$L_2^r(M_\rho)$	0.71 ± 0.27	1.49	1.35 ± 0.3
L_3	-2.72 ± 1.12	-3.18	-3.5 ± 1.1
$L_4^r(M_\rho)$	0	0	-0.3 ± 0.5
$L_5^r(M_\rho)$	0.91 ± 0.15	1.46	1.4 ± 0.5
$L_6^r(M_\rho)$	0	0	-0.2 ± 0.3
L_7	-0.32 ± 0.15	-0.49	-0.4 ± 0.2
$L_8^r(M_\rho)$	0.62 ± 0.2	1.00	0.9 ± 0.3

TABLE I. Different sets of chiral parameters $\times 10^3$. The second and third columns come from an $O(p^6)$ and $O(p^4)$ analysis of K_{l4} decays [42], respectively. Note that L_4^r and L_6^r are set to zero. In the third column L_1^r, L_2^r, L_3 are taken from [43] and the rest from [2] (L_4^r and L_6^r are estimated from the Zweig rule).

In Fig.2 we show the results of the IAM with the values given in the fourth column of Table I. The solid curve corresponds to the central values, whereas the shaded areas cover the uncertainty due to the error on the parameters. They have been obtained with a Monte-Carlo Gaussian sampling of 1000 choices of low energy constants for each \sqrt{s} , assuming the errors are uncorrelated. It is worth noticing that these error bands are so wide that the results for the other columns in Table I are rather similar, even for the central values. Qualitatively all of them look the same.

It can be noticed that the IAM results, even with the low energy parameters from standard ChPT, already provide distinct resonant shapes of the ρ , $f_0(980)$, K^* , and $a_0(980)$ (see Figs. 2.a, 2.b, 2.g, and 2.j, respectively). In addition, the IAM also provides two other extremely wide structures in the $(0, 0)$ $\pi\pi$ and $(1/2, 0)$ πK scattering amplitudes. They correspond to the σ (or $f_0(400 - 1200)$) and κ (see Figs. 2.b and 2.h). These structures are too wide to be considered as Breit-Wigner resonances, but they are responsible for the relatively high values of the phase shifts (the strength of the interaction) already near threshold. In the last years there has been a considerable discussion about the existence and properties of these two states (for references, see the scalar meson review in the PDG [45]). Since ChPT does not deal directly with quarks and gluons, it is very difficult to make any conclusive statement about the spectroscopic nature of these states (whether they are $q\bar{q}$, four quarks states, meson molecules, etc...) unless we make additional assumptions [44], which would then spoil much of the model independency of our approach, which is based just on chiral symmetry and unitarity. Nevertheless, the simplicity and remarkable results of this method gives a strong support, from the theoretical side, for the existence of both the σ and the κ . From previous works, it is known that the ChPT amplitudes unitarized with the IAM generate the poles in the second Riemann sheet associated with the

σ and the κ around $\sqrt{s_{pole}} \simeq 440 - i225$ MeV [8,9] and $\sqrt{s_{pole}} \simeq 770 - i250$ MeV [9], respectively. (Let us remember that since these states are very wide, the familiar relations $M \simeq \text{Re} \sqrt{s_{pole}}$ and $\Gamma \simeq -2\text{Im} \sqrt{s_{pole}}$ are very crude approximations). We have checked that similar results are obtained for the amplitudes of this work. These values have to be considered as estimates, since the uncertainties must be rather big, taking into account that the data in this channels are very conflictive (see Figs. 2 and 3). The fact that we are able to reproduce these states with parameters compatible with previous determinations is also a strong support for their masses and widths, which are in agreement with recent experimental determinations both for the σ and the κ [46].

To summarize, we have just shown how the present status of both the experimental data and the L_i determinations allows for a use of the IAM despite the approximations made on its derivation, like the poor description of the left cut commented above.

VII. IAM FIT TO THE SCATTERING DATA

Once we have seen that the IAM already describes the basic features of meson-meson scattering, we can proceed to fit the data in order to obtain a more accurate description. For that purpose we have used the MINUIT function minimization and error analysis routine from the CERN program library [47].

Our results are presented in Fig.3, whose different curves and bands can be understood as follows: As we have already seen when commenting the experiments in the previous section, and as it can be noticed in Figs.2 and 3, there are several incompatible sets of data for some channels. In the literature, this is usually solved by adding an extra systematic error until these values are compatible. We have made three fits by adding a 1%, 3% and 5% errors to the data on each channel. The continuous line corresponds to the 3% case and the resulting L_i values are listed in the second column of Table II. The shaded areas have been obtained again from a Monte-Carlo sampling using the L_i uncertainties given by MINUIT for this fit, which are listed on the third column of Table II. Let us remark that there would be almost no difference to the naked eye if we showed the fit with a 1% or a 5%, neither in the central continuous line nor in the shaded bands. Furthermore, the $\chi^2/d.o.f$ for any of these fits is always $O(1)$.

However, although the curves may almost remain unchanged when fitting with a different global systematic error, the values of the L_i come out somewhat different from each fit. This is an additional source of error on the L_i parameters, listed on the fourth column of Table II. It can be noticed that it dominates the uncertainty on the L_i . For illustration, the area between the dotted lines in Fig.3 corresponds to a Gaussian sampling of the chiral parameters with the two sources of error added in

quadrature.

By comparing the L_i^r from the IAM fit in Table II with those of previous ChPT determinations (in Table I), we see that there is a perfect agreement between them. This comparison of the complete IAM fit parameters is only possible now that we have the full $O(p^4)$ amplitudes, given in Appendix B, which are regularized and renormalized following the same scheme as standard ChPT. In particular, the agreement in the value of L_7 indicates that we are including the effects of the η' consistently.

	Fit+errors (curve in Fig.3)	MINUIT error (band in Fig.3)	From data systematic error
$L_1^r(M_\rho)$	0.56 ± 0.10	± 0.008	± 0.10
$L_2^r(M_\rho)$	1.21 ± 0.10	± 0.001	± 0.10
L_3	-2.79 ± 0.14	± 0.02	± 0.12
$L_4^r(M_\rho)$	-0.36 ± 0.17	± 0.02	± 0.17
$L_5^r(M_\rho)$	1.4 ± 0.5	± 0.02	± 0.5
$L_6^r(M_\rho)$	0.07 ± 0.08	± 0.03	± 0.08
L_7	-0.44 ± 0.15	± 0.003	± 0.15
$L_8^r(M_\rho)$	0.78 ± 0.18	± 0.02	± 0.18

TABLE II. Low energy constants obtained from an IAM fit to the meson-meson scattering data. The errors listed in the second column are obtained by adding in quadrature those of columns 3 and 4.

The threshold parameters (scattering lengths and slope parameters) obtained with the IAM are given in Table III for the low energy constants in the second column in Table II. The errors in Table III are obtained by a Gaussian sampling of the above low energy constants. Note that the experimental values of the threshold parameters have not been used as input in the fit, and the numbers we give are therefore predictions of the IAM. As we have anticipated before and Table III shows clearly, we are able to reproduce the low energy behavior with great accuracy. Let us then comment, for each different channel, on the results of the IAM fit:

Channel (I,J)=(1,1) The most striking feature of this channel is the $\rho(770)$ resonance, which, as it can be seen in Fig.3a, can be fitted with a great precision. This had already been achieved at $O(p^4)$ both with the single [8] and the coupled [11] channel formalisms. However, this is now achieved in a simultaneous fit with all the other channels, but since we are using the complete $O(p^4)$ expressions we have a good description of the high energy data without spoiling the scattering lengths listed in Table III.

This channel depends very strongly on $2L_1^r + L_3 - L_2^r$, and this combination can thus be fitted with great accuracy. The mass and width from a clear Breit-Wigner resonance can be obtained from the phase shift by means of

$$\delta_{IJ}(M_R) = 90^\circ \quad , \quad \Gamma_R = \frac{1}{M_R} \left(\frac{d\delta_{IJ}}{ds} \right)_{s=M_R^2}^{-1} . \quad (34)$$

For the (1,1) case we obtain $M_\rho = 775.7_{-3.3}^{+4.3}$ MeV and

$\Gamma_\rho = 135.5_{-9.0}^{+8.0}$ MeV, in perfect agreement with the values given in the PDG [45]. The errors correspond to a Gaussian sampling with the central values quoted in the second column of Table II and the MINUIT errors of the fit.

Finally, and just for illustration, the inelasticity prediction from the IAM is shown in Fig.3d. Note that the data values are so small and the claimed precision is so tiny that any other effect not considered in this work (like the 4π intermediate state) would yield a contribution beyond the precision we can expect to reach with the IAM. That is why they have been excluded from the fit.

Channel (I,J)=(0,0) There are three independent observables in this channel with data. Concerning the $\pi\pi$ scattering phase shift, plotted in Fig.3b, we can reproduce two resonant structures. First, there is the σ (or $f_0(400 - 1200)$), which corresponds to a broad bump in the phase shift, that gets as high as 50° not very far from threshold. This is not a narrow Breit Wigner resonance. Indeed it was shown in the IAM with just one channel [8], that it is possible to find an associated pole in the second Riemann sheet, quite far from the real axis. Second, we can nicely reproduce the shape of the $f_0(980)$ which corresponds to a narrow Breit-Wigner resonance although over a background phase provided by the σ , so that its mass and width cannot be read directly from Eq.(34).

Once more, it can be seen that the scattering lengths can also be reproduced simultaneously with the high energy data.

The next observable is the $\pi\pi \rightarrow K\bar{K}$ phase shift, Fig.3c, which can also be fitted neatly. Since we have included the $\eta\eta$ intermediate state, the fit is somewhat better than with just two channels above the two η threshold, as it was suggested in [11], but not as much as expected (this could be due to our crude treatment of $\eta - \eta'$ mixing, that we commented at the end of section II).

Finally, in Fig.3d, we show the inelasticity in the (0,0) channel. These are the most controversial sets of data, since there is a strong disagreement between several experiments (up to a factor of 2 in the overall normalization), as we have mentioned when commenting the data on this observable.

Channel (I,J)=(2,0) We have plotted the results in Fig.3.e. Since only the $\pi\pi$ state can have these quantum numbers, we are simply reproducing the single channel IAM formalism that already gave a very good description of this non-resonant channel [9]. Nevertheless, let us remark that it is now fitted simultaneously with all the other channels, and the value of the scattering length obtained from our fit is compatible with the experimental result and standard ChPT, see Table III.

In addition, once we have a description of this and the (0,0) channel, we can obtain the phase of the ϵ' parameter which measures direct CP violation in $K \rightarrow \pi\pi$ decays [48]. It is defined, in degrees, as follows:

$$\phi(\epsilon') = 90^\circ - (\delta_{00} - \delta_{20})_{s=M_K^2} . \quad (35)$$

Our result is $\phi(\epsilon') = 38 \pm 0.3$, where the error is obtained from a Gaussian sampling of the parameters listed in column 2 of Table II with the MINUIT errors on the third column. This is in very good agreement with the experimentally observed value of $\phi(\epsilon') = 43.5 \pm 7$. Standard ChPT [49] predicts 45 ± 6 .

Low energy K_{I4} decay data. There is no real improvement in the description of these low energy data in Fig.3f compared to ChPT, since standard ChPT is working very well at these energies. However, these very precise data at so low energies ensure that the parameters of our fit cannot be too different from those of standard ChPT. In addition, they are extremely important in the determination of the scattering lengths, in particular, of the controversial a_{00} .

Channel (I,J)=(1/2,1) As it happened in the (1,1) channel with the ρ , this channel is dominated by the $K^*(892)$. This is a distinct Breit-Wigner resonance that can be fitted very accurately with the IAM, see Fig.3g. From Eq.(34) we find $M_{K^*} = 889 \pm 5$ MeV and $\Gamma_{K^*} = 46 \pm 13$ MeV, in fairly good agreement with the PDG [45]. The errors have been obtained in the same way as for the ρ resonance in the (1,1) channel.

Channel (I,J)=(1/2,0) Due to the wide dispersion of experimental results, our fit yields a wide error band for this channel, as it can be seen in Fig.3h. Nevertheless, as it happened in the (0,0) channel, the phase shift is of the order of 50° not far for threshold, due to a wide bump similar to the σ in that channel. Here such a broad structure has been identified by different experimental and theoretical analysis [50,9,51,46] as the κ although there is still a controversy about its existence and origin [52], as it also happened with the σ . It is very similar to the σ , and hence it cannot be interpreted as a Breit-Wigner narrow resonance.

We also give in Table III the value for the scattering length of this channel, in good agreement with the experimental data, which nevertheless is not very well known.

Channel (I,J)=(3/2,0) Since only πK can have these quantum numbers, this is once more the IAM with a single channel, which already provided a very good description [8]. We show in Fig.3i the results of the global fit for this channel, as well as the corresponding scattering length in Table III.

Channel (I,J)=(1,0) In our global fit, the data in this channel, see Fig.3.j, are reproduced using Eq.(33). The shape of the $a_0(980)$ is neatly reproduced in the mass distribution. In order to compare the value of the normalization constant c with experiment, we also show in Fig.4 the result of applying the IAM with the parameters obtained from our fit to the experimental data obtained from $K^-p \rightarrow \Sigma^+(1385)\pi\eta$ and $K^-p \rightarrow \Sigma^+(1385)K\bar{K}$ [53]. These data have not been included in our fit since they do not have error bars, but it can be seen that the IAM provides a good description. Once again we are using a formula like Eq.(33), but with a constant different from that for Fig.3.j and no background. Our result is $c = 63 \pm 15 \mu\text{b}/\text{GeV}$, to be compared with the values

quoted in [53] where c was taken from 73 to $165 \mu\text{b}/\text{GeV}$.

Channel (I,J)=(0,1) Finally, we show in Fig.5 the results for the modulus of the amplitude in the (0,1) channel. In this case, there is only one meson-meson scattering channel, namely $K\bar{K} \rightarrow K\bar{K}$. Therefore, we can only apply the single channel IAM, and in so doing we find a pole at approximately 935 MeV in the real axis. The width of this resonance is zero, since within our approach it can only couple to $K\bar{K}$ and its mass is below the two kaon threshold. One is tempted to identify this resonance with the $\phi(1020)$ meson, but in fact it can only be related to its octet part ω_8 . The reason is that the singlet part ω_1 is SU(3) symmetric and it does not couple to two mesons since their spatial function has to be antisymmetric. Consequently we can only associate the resonance obtained with the IAM to the octet ω_8 [9,54]. The position of the pole seems consistent with an intermediate mass between the $\phi(1020)$ and the $\omega(770)$. This state had also been found when using the IAM with the incomplete chiral amplitudes [9], and it had been used later to study the $\phi \rightarrow \pi\pi$ decay within a chiral unitary approach [54]. The fact that we find it here again confirms that it is not an artifact of the approximations used in [9]. In addition although the amplitudes used here are complete up to $O(p^4)$ and the fit is rather different, it appears almost at the same place, which supports the soundness of the results in [9].

	Experiment	IAM fit	ChPT $\mathcal{O}(p^4)$	ChPT $\mathcal{O}(p^6)$
a_{00}	0.26 ± 0.05	$0.231^{+0.003}_{-0.006}$	0.20	0.219 ± 0.005
b_{00}	0.25 ± 0.03	0.30 ± 0.01	0.26	0.279 ± 0.011
a_{20}	-0.028 ± 0.012	$-0.0411^{+0.0009}_{-0.001}$	-0.042	-0.042 ± 0.01
b_{20}	-0.082 ± 0.008	-0.074 ± 0.001	-0.070	-0.0756 ± 0.0021
a_{11}	0.038 ± 0.002	0.0377 ± 0.0007	0.037	0.0378 ± 0.0021
$a_{1/20}$	$0.13 \dots 0.24$	$0.11^{+0.06}_{-0.09}$	0.17	
$a_{3/20}$	$-0.13 \dots -0.05$	$-0.049^{+0.002}_{-0.003}$	-0.5	
$a_{1/21}$	$0.017 \dots 0.018$	0.016 ± 0.002	0.014	
a_{10}		$0.15^{+0.07}_{-0.11}$	0.0072	

TABLE III. Scattering lengths a_{IJ} and slope parameters b_{IJ} for different meson-meson scattering channels. The experimental data come from [10,55], the one loop results from [5,8,10] and those at two loops from [42]. We are using the definitions and conventions given in those references. Let us remark that our one-loop IAM results are closer to those of two-loop ChPT, although the IAM depends on much less parameters than the $O(p^6)$ ChPT.

Finally, we have also added in Fig.3 a dashed line that corresponds to the result with the central values of the parameters in the second column of Table II, but where we have used the one-channel IAM at energies where there is only one state available, the two-channel IAM when there are two, etc... As we commented at the end of section IV, this approach ensures exact unitarity at all energies, but we can see that it generates a discontinuity at each threshold. The results are compatible within the

wider error bands with the previous IAM fit (the space between dotted lines). This was expected since, as we have already commented, the difference between the two approaches is of the order of a few percent, which is also the order of magnitude of the systematic error added to the data for the fit. Of course, it is possible to obtain also a fit with this method, as it was done in [8] and the resulting parameters are still compatible with those listed in Table III.

VIII. CONCLUSIONS

In this work we have completed the calculation of the lightest octet meson-meson scattering amplitudes within Chiral Perturbation Theory (ChPT) at one loop. We have calculated three new amplitudes, $\eta\eta \rightarrow \eta\eta$, $K\eta \rightarrow K\eta$ and $K\eta \rightarrow K\pi$ but we have also recalculated the other five independent amplitudes, checking and revising previous results. The full expressions are given in Appendix B in a unified notation, using dimensional regularization and the $\overline{MS} - 1$ renormalization scheme, which is the usual one within ChPT. All the meson-meson scattering partial waves below 1200 MeV, with definite isospin I and angular momentum J , can be expressed in terms of those eight amplitudes.

Since ChPT is a low energy theory, the one loop amplitudes have to be unitarized in order to reach energies as high as 1200 MeV (and in particular the two kaon threshold). For that purpose we have applied the coupled channel Inverse Amplitude Method, which ensures unitarity for coupled channels and it is also able to generate resonances and their associated poles, without introducing any additional parameter. In addition, it respects the chiral expansion at low energies, in our case up to $O(p^4)$. Thus, we have shown how it is possible to describe simultaneously the data on the $(I, J) = (0, 0), (1, 1), (2, 0), (1, 0), (1/2, 0), (1/2, 1), (3/2, 0)$ meson-meson channels below 1200 MeV, which correspond to 20 different reactions. We also describe seven resonant shapes, namely, the σ , $\rho(770)$, $K^*(892)$, κ , $f_0(980)$, $a_0(980)$ and the octet ϕ .

This description is achieved with values for the low energy constants which are perfectly compatible with previous determinations obtained using standard ChPT and low energy data. This comparison is only possible as far as we now have the complete $O(p^4)$ expression for all the amplitudes in the standard ChPT scheme. Indeed, with the present determinations of standard ChPT, we already find the resonance shapes and we obtain the most distinct features of each channel, although with big uncertainties due to the present knowledge of the chiral parameters.

Nevertheless, we have performed a fit of our unitarized amplitudes to the meson-meson data and we have obtained a very accurate description not only of the resonance region, but also of the low energy data, and in particular of the scattering lengths. We have also paid par-

ticular attention to the uncertainties and errors in our description, which have been estimated with Monte-Carlo samplings of the fitted chiral parameters within their resulting error bars.

Summarizing, we have extended and completed previous analysis of these techniques in the meson sector so that we believe that our present work could be useful for further phenomenological applications.

ACKNOWLEDGMENTS.

We are very grateful to J.A. Oller for his comments, clarifications and discussions over almost every issue addressed in this paper. We also thank J.Nieves and E.Ruiz-Arriola for providing and explaining to us the Monte-Carlo code used to generate the error bands. In addition, we have profited from interesting discussions with A. Dobado and E. Oset. We acknowledge partial support from the Spanish CICYT projects AEN97-1693, and FPA2000-0956, PB98-0782 and BFM2000-1326.

APPENDIX A: USEFUL FORMULAE

Here we will give the main results and definitions of the different functions coming from the one-loop ChPT calculation. We are following the notation and conventions of [3].

When calculating the ChPT amplitudes, the typical loop integrals that appear are, on the one hand, the tadpole integral, i.e, the Feynman boson propagator evaluated at $x = 0$:

$$\int \frac{d^d q}{(2\pi)^d} \frac{i}{q^2 - M_i^2} = 2M_i^2 \lambda + \frac{M_i^2}{16\pi^2} \log \frac{M_i^2}{\mu^2} \quad (\text{A1})$$

where μ is the renormalization scale, $i = \pi, K, \eta$, and we have extracted its divergent part for $d \rightarrow 4$, with λ given in (5). On the other hand, the integrals coming from diagrams (a),(b) and (c) in Figure 1 is:

$$J_{PQ}(p^2) = -i \int \frac{d^d q}{(2\pi)^d} \frac{1}{[q^2 - M_P^2][(q-p)^2 - M_Q^2]} \quad (\text{A2})$$

where $P, Q = \pi, K, \eta$ and whose divergent contribution in dimensional regularization can be separated as

$$J_{PQ}(s) = J_{PQ}(0) + \bar{J}_{PQ}(s) + \mathcal{O}(d-4) \quad (\text{A3})$$

where

$$\begin{aligned} J_{PQ}(0) &= -2\lambda - \frac{1}{16\pi^2} \frac{1}{\Delta} \left[M_P^2 \log \frac{M_P^2}{\mu^2} - M_Q^2 \log \frac{M_Q^2}{\mu^2} \right] \\ \bar{J}_{PQ}(s) &= \frac{1}{32\pi^2} \left[2 + \left(\frac{\Delta}{s} - \frac{\Sigma}{\Delta} \right) \log \frac{M_Q^2}{M_P^2} \right. \\ &\quad \left. - \frac{\nu(s)}{s} \log \frac{(s + \nu(s))^2 - \Delta^2}{(s - \nu(s))^2 - \Delta^2} \right] \end{aligned} \quad (\text{A4})$$

and

$$\begin{aligned}\Delta &= M_P^2 - M_Q^2 \\ \Sigma &= M_P^2 + M_Q^2 \\ \nu^2(s) &= \left[s - (M_P + M_Q)^2 \right] \left[s - (M_P - M_Q)^2 \right]\end{aligned}$$

For the case of a single mass $M_P = M_Q$, the above integrals read

$$\begin{aligned}J_{PP}(s) &= -2\lambda - \frac{1}{16\pi^2} \left(1 + \log \frac{M_P^2}{\mu^2} \right) + \bar{J}_{PP}(s) \\ \bar{J}_{PP}(s) &= \frac{1}{16\pi^2} \left[2 + \sigma(s) \log \frac{\sigma(s) - 1}{\sigma(s) + 1} \right]\end{aligned}\quad (\text{A5})$$

with

$$\sigma(s) = (1 - 4M_P^2/s)^{1/2} \quad (\text{A6})$$

Note that the above integrals have the correct unitarity structure in the right cut which extends on the real axis from $s = (M_P + M_Q)^2$ to infinity. In fact, all the integrals appearing to one loop in ChPT can be expressed in terms of the tadpole and \bar{J} integrals above [3]. However, it is customary to express the results also in terms of:

$$\bar{\bar{J}}_{PQ}(s) \equiv \bar{J}(s) - s\bar{J}'(0) \quad (\text{A7})$$

where, from (A4) one has,

$$\bar{J}'(0) = \frac{1}{32\pi^2} \left[\frac{\Sigma}{\Delta^2} + 2 \frac{M_P^2 M_Q^2}{\Delta^3} \log \frac{M_Q^2}{M_P^2} \right] \quad (\text{A8})$$

From the above definitions it is easy to check that the functions $\bar{J}(s)/s$ and $\bar{\bar{J}}(s)/s^2$ have well-defined limits as $s \rightarrow 0$.

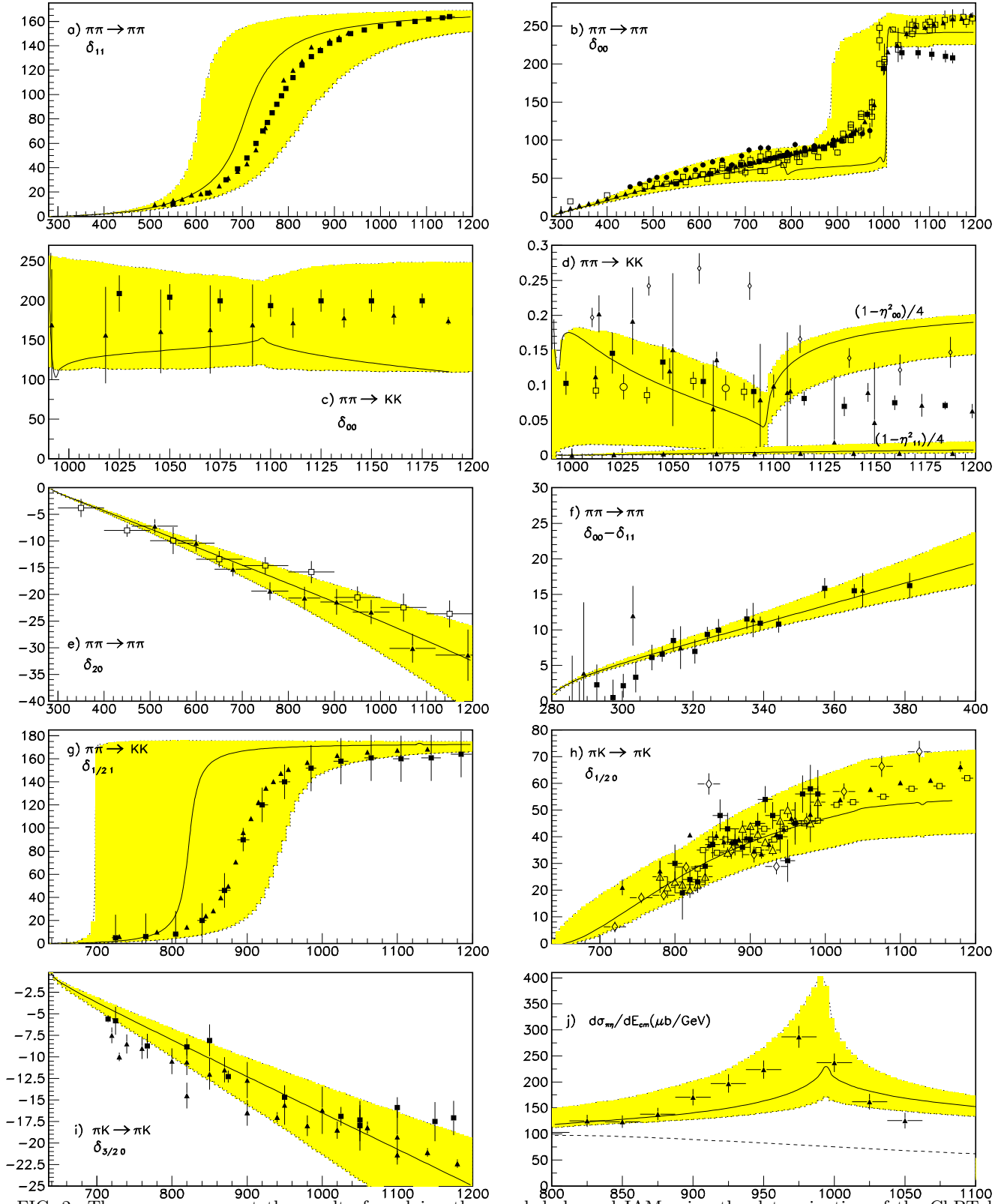


FIG. 2. The curves represent the result of applying the coupled channel IAM using the determination of the ChPT low energy constant given in the fourth column of Table 1. The shaded area covers the uncertainty due to the errors in those determinations (assuming they were totally uncorrelated).

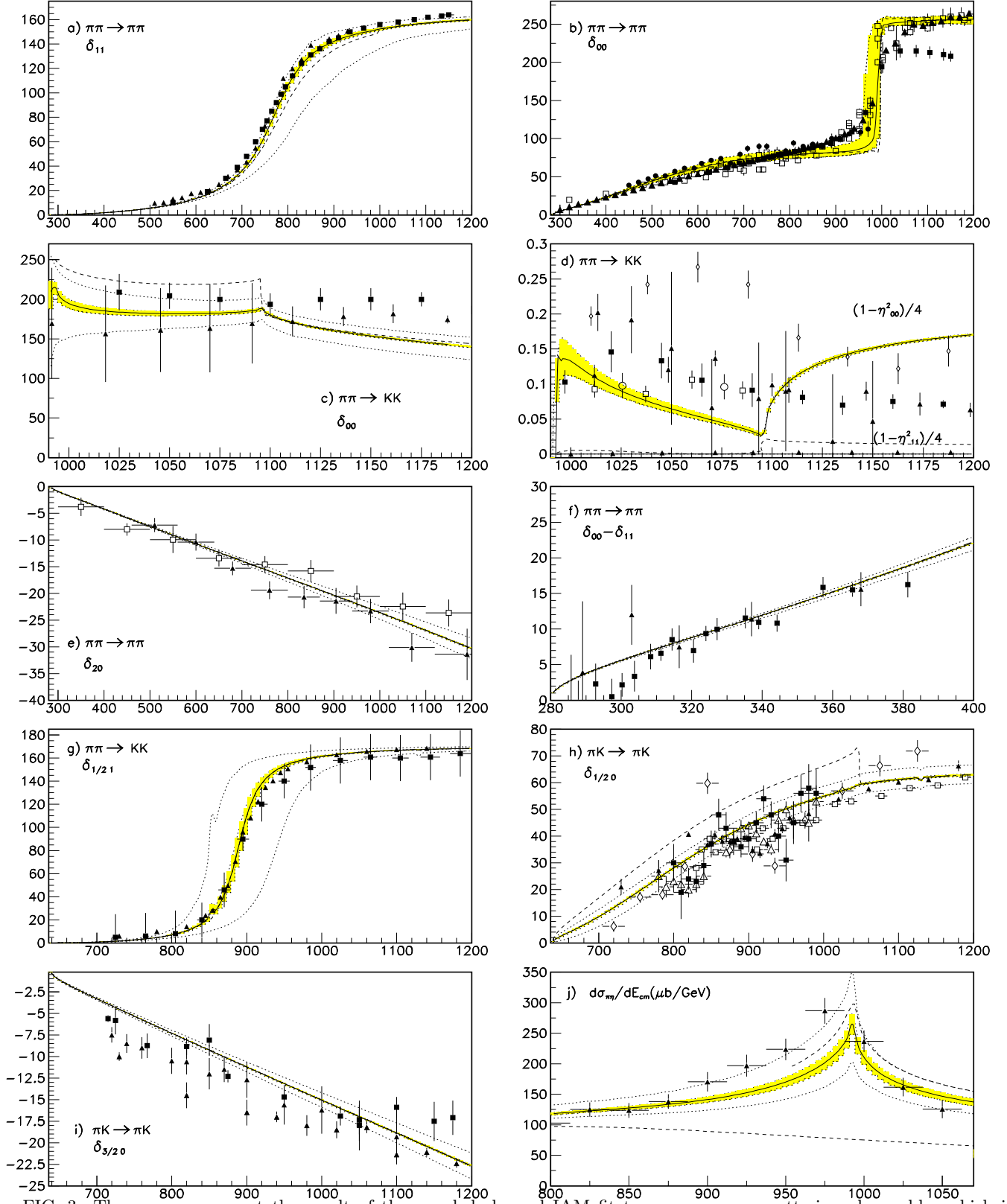


FIG. 3. The curves represent the result of the coupled channel IAM fit to meson-meson scattering observables which is described in the text. The shaded area covers only the uncertainty due to the statistical errors in the L_i parameters obtained from MINUIT (assuming they were uncorrelated). The area between dotted lines corresponds to the error bands including in the L_i the systematic error added to the data (see text for details). Finally, the dashed line corresponds to the use of the one channel IAM when only one channel is accessible, but keeping the same parameters of the previous fit.

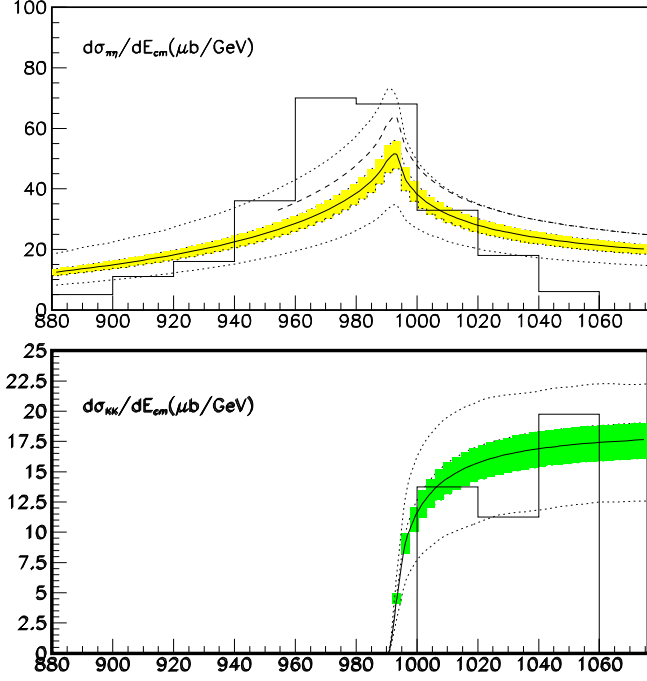


FIG. 4. We show the effective mass distributions of the two mesons in the final state of $K^-p \rightarrow \Sigma^+(1385)\pi\eta$ (top) and $K^-p \rightarrow \Sigma^+(1385)K\bar{K}$ (bottom), the data come from [53]. The curves and bands are as in Fig.3

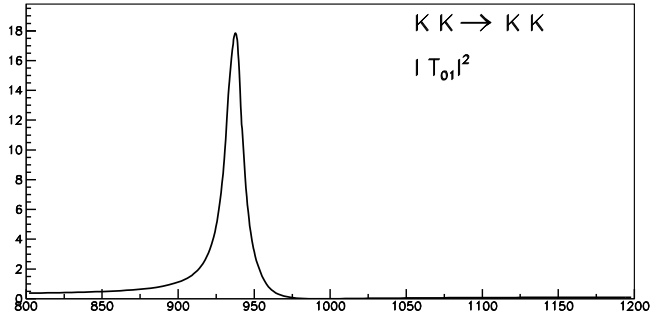


FIG. 5. We show the modulus of the $(I, J) = (0, 1)$ $K\bar{K} \rightarrow K\bar{K}$ amplitude. The pole around 935 can be identified with the octet ω_8 (see text for details). Although that cannot be shown in a plot, the modulus of the amplitude actually becomes infinite.

APPENDIX B: ONE LOOP AMPLITUDES FROM CHPT

Here we list the expressions of the eight independent meson-meson scattering amplitudes to one loop in ChPT. We have carefully checked the scale independence and perturbative exact unitarity (see section III). Note that we have used eq.(9) to write all the f_K and f_η in terms of f_π , L_4^r and L_5^r , in order to ensure ‘‘exact’’ perturbative unitarity, eq.(27). Let us first give the three amplitudes that had never appeared in the literature in any form:

For $\eta\eta \rightarrow \eta\eta$:

$$\begin{aligned}
T(s, t, u) = & \frac{16M_K^2 - 7M_\pi^2}{9f_\pi^2} + \frac{\mu_\pi}{9f_\pi^2} \{7M_\pi^2 - 48M_\eta^2\} - \frac{\mu_K}{18f_\pi^2 M_K^2} \{81[t^2 - su - 4tM_\eta^2] + 14M_\pi^4 - 48M_\pi^2 M_\eta^2\} \\
& + 378M_\eta^4 - \frac{\mu_\eta}{3f_\pi^2 M_\eta^2} \{M_\pi^4 - 8M_\pi^2 M_\eta^2 + 24M_\eta^4\} + \frac{4}{f_\pi^4} (2L_1^r + 2L_2^r + L_3) \{s^2 + t^2 + u^2 - 4M_\eta^4\} \\
& - \frac{8}{3f_\pi^4} \{12M_\eta^4 L_4^r + (3M_\pi^4 - 10M_\pi^2 M_\eta^2 + 13M_\eta^4) L_5^r - 36M_\eta^4 L_6^r - 24(M_\pi^4 - 3M_\pi^2 M_\eta^2 + 2M_\eta^4) L_7 \\
& - 6L_8^r (2M_\pi^4 - 6M_\pi^2 M_\eta^2 + 7M_\eta^4)\} - \frac{1}{192\pi^2 f_\pi^4} \{27(t^2 - su - 4tM_\eta^2) + 16(23M_\eta^4 - 22M_K^2 M_\eta^2 + 10M_K^4)\} \\
& + \frac{1}{6f_\pi^4} \left\{ \frac{1}{27} (16M_K^2 - 7M_\pi^2)^2 \bar{J}_{\eta\eta}(s) + M_\pi^4 \bar{J}_{\pi\pi}(s) + \frac{1}{12} (9s - 2M_\pi^2 - 6M_\eta^2)^2 \bar{J}_{KK}(s) + [s \leftrightarrow t] + [s \leftrightarrow u] \right\}.
\end{aligned} \tag{B1}$$

For $\bar{K}^0\eta \rightarrow \bar{K}^0\eta$

$$\begin{aligned}
T(s, t, u) = & \frac{9t - 6M_\eta^2 - 2M_\pi^2}{12f_\pi^2} - \frac{2L_5^r}{3f_\pi^4} [3M_\pi^4 + 12M_\eta^4 + M_\pi^2(5M_\eta^2 - 9t)] \\
& + \frac{1}{3f_\pi^4} \left\{ 2(12L_1^r + 5L_3^r)(2M_K^2 - t)(2M_\eta^2 - t) + (12L_2^r + L_3) \left[(s - M_K^2 - M_\eta^2)^2 + (u - M_K^2 - M_\eta^2)^2 \right] \right\} \\
& + \frac{4}{f_\pi^4} \{8(L_6^r - L_4^r)M_K^2 M_\eta^2 + 2L_7(M_\pi^4 - 4M_\pi^2 M_\eta^2 + 3M_\eta^4) + L_8^r(M_\pi^4 - 3M_\pi^2 M_\eta^2 + 6M_\eta^4) + 2L_4^r t(M_\eta^2 + M_K^2)\} \\
& - \frac{\mu_\pi}{48f_\pi^2 (M_K^2 - M_\eta^2)} \{2M_K^2 [26M_\eta^2 + 69t] - 84M_K^4 + 3[16M_\eta^4 - 50tM_\eta^2 + (s - u)^2]\} \\
& - \frac{\mu_K}{72f_\pi^2 M_K^2 (M_K^2 - M_\eta^2)} \{92M_K^6 - 81M_\eta^2 t^2 - 60M_K^4 [3t + M_\eta^2] + 18M_K^2(5t^2 - 2su + 6tM_\eta^2 + 8M_\eta^4)\} \\
& + \frac{\mu_\eta}{144f_\pi^2 M_\eta^2 (M_K^2 - M_\eta^2)} \{144tM_K^4 - 128M_K^6 + [27(s - u)^2 - 486tM_K^2 + 428M_K^4] M_\eta^2 \\
& + 2[153t - 166M_K^2] M_\eta^4 + 144M_\eta^6\} + \frac{1}{2304f_\pi^4 \pi^2} \{116M_K^4 + M_K^2 [184M_\eta^2 - 153t] \\
& - 9[10t^2 + 2su - 3tM_\eta^2 + 4M_\eta^4]\} + \frac{t\bar{J}_{KK}(t)(9t - 2M_\pi^2 - 6M_\eta^2)}{16f_\pi^4} + \frac{\bar{J}_{\eta\eta}(t)(9t - 2M_\pi^2 - 6M_\eta^2)(16M_K^2 - 7M_\pi^2)}{216f_\pi^4} \\
& + \frac{t\bar{J}_{\pi\pi}(t)M_\pi^2}{8f_\pi^4} + \frac{1}{32f_\pi^4} \left\{ \frac{\bar{J}_{K\eta}(s)}{9} [27s(s - u) + 189M_K^4 + 8M_\pi^4 + 54uM_\eta^2 + 45M_\eta^4 + 12M_\pi^2(3s - 2M_\eta^2) \right. \\
& - 18M_K^2(6s - 3u + 4M_\pi^2 + 9M_\eta^2)] + \frac{\bar{J}_{K\pi}(s)}{9} [27s(s - u) + 29M_K^4 + 11M_\pi^4 + 18M_\eta^4 \\
& + 2M_K^2(18s + 27u - 47M_\pi^2 - 78M_\eta^2) + 6M_\pi^2(9u - 6s + 8M_\eta^2)] - \frac{\bar{J}_{K\pi}(s)}{s} [M_K^4(3u + 14M_\pi^2 - 8M_\eta^2) \\
& + 2M_K^6 - 2M_K^2 M_\pi^2(3u + 5M_\pi^2 + 4M_\eta^2) + M_\pi^2(6M_\eta^4 + M_\pi^2(3u + 4M_\eta^2))] \\
& \left. + \frac{\bar{J}_{K\eta}(s)}{s} (M_K^2 - M_\eta^2)^2 (4M_\pi^2 - 18M_K^2 - 6M_\eta^2 - 3u) \right. \\
& \left. + 6(M_K^2 - M_\eta^2)^2 \frac{\bar{J}_{K\pi}(s)(M_K^2 - M_\pi^2)^2 + \bar{J}_{K\eta}(s)(M_K^2 - M_\eta^2)^2}{s^2} + [s \leftrightarrow u] \right\}.
\end{aligned} \tag{B2}$$

For $\bar{K}^0\eta \rightarrow \bar{K}^0\pi^0$:

$$\begin{aligned}
T(s, t, u) = & \frac{8M_K^2 + 3M_\eta^2 + M_\pi^2 - 9t}{12\sqrt{3}f_\pi^2} + \frac{\mu_\pi}{48\sqrt{3}f_\pi^2(M_K^2 - M_\pi^2)} \{27s^2 + 18su + 27u^2 + 174tM_K^2\} \\
& - 292M_K^4 + 12(5M_K^2 - 6t)M_\pi^2 - 32M_\pi^4 - \frac{\mu_K}{24\sqrt{3}f_\pi^2M_K^2(M_K^2 - M_\pi^2)} \{9t^2M_\pi^2 + 24M_K^6 \\
& + 4M_K^4(17M_\pi^2 - 15t) + 2M_K^2[9(s-u)^2 + 6tM_\pi^2 - 22M_\pi^4]\} - \frac{\mu_\eta}{16\sqrt{3}f_\pi^2(M_K^2 - M_\eta^2)} \{3(s-u)^2 \\
& + 2(3t - 14M_K^2 + 10M_\eta^2)(M_K^2 - 2M_\eta^2)\} + \frac{1}{256\sqrt{3}\pi^2f_\pi^4} \{2(2s+u)(s+2u) - 192M_K^4 - 23tM_\eta^2 - 16M_\eta^4 \\
& + 5M_K^2(13t + 24M_\eta^2)\} - \frac{L_3}{\sqrt{3}f_\pi^4} \{s^2 + 4su + u^2 - 30M_K^4 - 2tM_\eta^2 + 2M_\eta^4 + 6M_K^2(t + 2M_\eta^2)\} \\
& + \frac{1}{\sqrt{3}f_\pi^4} \{3M_\pi^4[L_5^r - 2(2L_7 + L_8^r)] + M_\eta^4[6(2L_7 + L_8^r) - L_5^r] - 6L_5^rM_\pi^2(t - M_\eta^2)\} \\
& - \frac{9t - 8M_K^2 - M_\pi^2 - 3M_\eta^2}{144\sqrt{3}f_\pi^4} [3t\bar{J}_{KK}(t) + 4M_\pi^2\bar{J}_{\pi\eta}(t)] + \frac{1}{288\sqrt{3}f_\pi^4} \{\bar{J}_{K\eta}(s)[27s(u-s) - 45M_K^4 + 14M_\pi^4 \\
& - 6M_\eta^2(9u + 7M_\pi^2) - 9M_\eta^4 + M_K^2(36s - 54u + 22M_\pi^2 + 156M_\eta^2)] + 3\bar{J}_{K\pi}(s)[29M_K^4 + 7M_\pi^4 \\
& + 3s(9s + 3u - 4M_\eta^2) - 2M_K^2(16s + 9u - 18M_\pi^2 + 3M_\eta^2) - M_\pi^2(40s + 18u - 30M_\eta^2)] \\
& + 9\frac{\bar{J}_{K\eta}(s)}{s}(M_K^2 - M_\eta^2)[10M_K^4 + 2M_\pi^4 - M_\eta^2(3u + 8M_\pi^2) + M_K^2(3u - 12M_\pi^2 + 8M_\eta^2)] \\
& + 9\frac{\bar{J}_{K\pi}(s)}{s}(M_K^2 - M_\pi^2)^2(3u - 2M_K^2 + 2M_\pi^2) - \frac{54\bar{\bar{J}}_{K\eta}(s)}{s^2}(M_K^2 - M_\pi^2)(M_K^2 - M_\eta^2)^3 \\
& - \frac{54\bar{\bar{J}}_{K\pi}(s)}{s^2}(M_K^2 - M_\pi^2)^3(M_K^2 - M_\eta^2) + [s \leftrightarrow u]\}.
\end{aligned} \tag{B3}$$

Apart from the above three amplitudes, we have recalculated the other independent five. The reason is threefold. First, we wanted them to satisfy exact perturbative unitarity to apply the simplest IAM formulae. This was not the case of all the calculations in the literature, even when considering the one-channel case. Second, there have been several unfortunate misprints and errata in the published formulae (including some errata made by one of the authors). Finally we would like to have a self-contained description of the one-loop calculation, together with all the resulting formulae. Nevertheless, when compared with previous analysis, our results are not exactly the same because we have chosen to express the amplitudes in terms of only one physical decay constant f_π , and we have only used the Gell-Mann-Okubo relation to simplify masses if it did not affected the exact perturbative unitarity relation. Apart from corrections, the differences are $O(p^6)$. The first amplitude to appear in the literature was $\pi^+\pi^- \rightarrow \pi^0\pi^0$, although in SU(2) [2]. However, we have been able to check also with the SU(3) calculation [10]. The result, following the notation in Appendix A, is:

$$\begin{aligned}
T(s, t, u) = & \frac{s - M_\pi^2}{f_\pi^2} - \frac{\mu_\pi}{3f_\pi^2M_\pi^2} \{4s^2 - 4tu - 4sM_\pi^2 + 9M_\pi^4\} - \frac{\mu_K}{6f_\pi^2M_K^2} \{s^2 - tu + 2sM_\pi^2\} - \frac{\mu_\eta M_\pi^4}{9f_\pi^2M_\eta^2} \\
& + \frac{4}{f_\pi^4} \{(2L_1^r + L_3)(s - 2M_\pi^2)^2 + L_2^r[(t - 2M_\pi^2)^2 + (u - 2M_\pi^2)^2]\} \\
& + \frac{8M_\pi^2}{f_\pi^4} \{(2L_4^r + L_5^r)s + 2(2L_6^r + L_8^r - 2L_4^r - L_5^r)M_\pi^2\} \\
& + \frac{1}{576\pi^2f_\pi^4} \{30(M_\pi^2 - s)s + 21tu - 56M_\pi^4\} + \frac{1}{2f_\pi^4} \left\{ \frac{s^2\bar{J}_{KK}(s)}{4} + \frac{M_\pi^4\bar{J}_{\eta\eta}(s)}{9} + (s^2 - M_\pi^4)\bar{J}_{\pi\pi}(s) \right\} \\
& + \frac{1}{6f_\pi^4} \left\{ \frac{(t - 4M_K^2)(2s + t - 4M_\pi^2)\bar{J}_{KK}(t)}{4} + [t(t-u) - 2M_\pi^2(t - 2u + M_\pi^2)]\bar{J}_{\pi\pi}(t) + [t \leftrightarrow u] \right\}.
\end{aligned} \tag{B4}$$

The $K^+\pi^+ \rightarrow K^+\pi^+$ one loop calculation was first given in [10]. It was correct up to $O(p^4)$ but when expressed in terms of physical constants it did not satisfy exact perturbative unitarity. One of the authors gave an expression satisfying that relation [8], but there was also a typographical error in that reference. Our corrected result, expressed just in terms of f_π is:

$$T^{3/2}(s, t, u) = \frac{M_K^2 + M_\pi^2 - s}{2f_\pi^2} + \frac{2}{f_\pi^4} \left\{ (4L_1^r + L_3)(t - 2M_K^2)(t - 2M_\pi^2) + (2L_2^r + L_3)(u - M_K^2 - M_\pi^2)^2 \right\} \tag{B5}$$

$$\begin{aligned}
& + 2L_2^r (s - M_K^2 - M_\pi^2)^2 + 4L_4^r [tM_\pi^2 + M_K^2 (t - 4M_\pi^2)] - 2L_5^r M_\pi^2 (s + M_K^2 - M_\pi^2) \\
& + 8(2L_6^r + L_8^r) M_K^2 M_\pi^2 \} + \frac{\mu_\pi}{24f_\pi^2 M_\pi^2 (M_\pi^2 - M_K^2)} \{ 2M_K^2 (7s + 5u - 12M_K^2) (2M_\pi^2 - t) \\
& - [26s^2 + 21su + 25u^2 - 3M_K^2 (s + 5u + 16M_K^2)] M_\pi^2 + (85s + 53u - 78M_K^2) M_\pi^4 - 66M_\pi^6 \} \\
& + \frac{\mu_K}{12f_\pi^2 M_K^2 (M_\pi^2 - M_K^2)} \{ 42M_K^6 - M_\pi^2 (5s + 4u - 9M_\pi^2) (2M_K^2 - t) + 4M_K^4 (12M_\pi^2 - 13s - 8u) \\
& + M_K^2 [11s^2 + 12su + 7u^2 - 3M_\pi^2 (s - u + 8M_\pi^2)] \} + \frac{\mu_\eta}{72f_\pi^2 M_\eta^2 (M_\eta^2 - M_\pi^2)} \{ 41M_\pi^6 - 18(s + u) M_\pi^4 \\
& + [36(s - u)u + 9(s + 5u) M_\pi^2 - 59M_\pi^4] M_\eta^2 - 3[9(5s + u) - 43M_\pi^2] M_\eta^4 + 81M_\eta^6 \} \\
& + \frac{1}{1152f_\pi^4 \pi^2} \{ 3(s - 10t)t - 6su - 3u^2 - 27M_K^4 + M_K^2 (30s - 3t + 21u - 34M_\pi^2) - 3M_\pi^2 (t - 2s - 3u + M_\pi^2) \} \\
& - \frac{\bar{J}_{K\pi}(u)}{16f_\pi^4} \{ (s - 5u)u + 5M_K^4 - 2(s - 2u) M_\pi^2 + 5M_\pi^4 - 2M_K^2 (s - 2u + 5M_\pi^2) \} \\
& + \frac{\bar{J}_{\pi\pi}(t)}{24f_\pi^4} \{ t(5t - 2s + 2M_K^2) + (8s + 3t - 8M_K^2) M_\pi^2 - 8M_\pi^4 \} - \frac{\bar{J}_{\eta\eta}(t)M_\pi^2}{72f_\pi^4} [2M_\pi^2 + 6M_\eta^2 - 9t] \\
& + \frac{\bar{J}_{KK}(t)}{24f_\pi^4} \{ M_K^2 (4s + 3t - 4M_\pi^2) + t(4t - s + M_\pi^2) - 4M_K^4 \} + \frac{\bar{J}_{K\eta}(u)}{432f_\pi^4} \{ 2M_K^2 (27s + 18u - 74M_\pi^2 - 51M_\eta^2) \\
& + 29M_K^4 + 38M_\pi^4 - M_\pi^2 (36u - 48M_\eta^2) - 9(3(s - u)u - 6sM_\eta^2 + M_\eta^4) \} + \frac{\bar{J}_{K\pi}(s)}{4f_\pi^4} (M_K^2 + M_\pi^2 - s)^2 \\
& - \frac{\bar{J}_{K\eta}(u)}{48f_\pi^4 u} \{ 2M_K^6 + 10M_\pi^4 M_\eta^2 + 3sM_\eta^4 + M_K^4 (3s - 4M_\pi^2 + 10M_\eta^2) - 2M_K^2 (2M_\pi^4 + (3s + 4M_\pi^2) M_\eta^2 + 3M_\eta^4) \} \\
& - (M_K^2 - M_\pi^2)^2 \frac{\bar{J}_{K\pi}(u) (s - 2M_K^2 - 2M_\pi^2)}{16f_\pi^4 u} + (M_K^2 - M_\pi^2)^2 \frac{(M_K^2 - M_\eta^2)^2 \bar{J}_{K\eta}(u) + (M_K^2 - M_\pi^2)^2 \bar{J}_{K\pi}(u)}{8f_\pi^4 u^2}.
\end{aligned}$$

The one-loop $\pi^0\eta \rightarrow \pi^0\eta$ amplitude was calculated in [10]. We give here the result expressed in terms of physical quantities:

$$\begin{aligned}
T(s, t, u) &= \frac{M_\pi^2}{3f_\pi^2} - \frac{(13M_\pi^4 + 6t(M_\pi^2 - M_\eta^2) - 9M_\pi^2 M_\eta^2) \mu_\pi}{9f_\pi^2 (M_\pi^2 - M_\eta^2)} + \frac{(M_\pi^6 - M_\pi^4 M_\eta^2 + 4M_\pi^2 M_\eta^4) \mu_\eta}{9f_\pi^2 M_\eta^2 (M_\pi^2 - M_\eta^2)} \quad (B6) \\
& - \frac{\mu_K}{6f_\pi^2 M_K^2} \{ 20M_\pi^2 (t - 3M_\eta^2) - 25M_\pi^4 + 3[3(s^2 + su + u^2) + 8tM_\eta^2 - 9M_\eta^4] \} \\
& + \frac{4}{f_\pi^4} \{ 2(L_1^r + L_3/6)(t - 2M_\pi^2)(t - 2M_\eta^2) + (L_2^r + L_3/3)[(s - M_\pi^2 - M_\eta^2)^2 + (u - M_\pi^2 - M_\eta^2)^2] \} \\
& + \frac{8}{f_\pi^4} \{ [t(M_\pi^2 + M_\eta^2) - 4M_\pi^2 M_\eta^2] L_4^r + 2(2L_6^r - L_5^r/3)M_\pi^2 M_\eta^2 + 4L_7 M_\pi^2 (M_\pi^2 - M_\eta^2) + 2L_8^r M_\pi^4 \} \\
& + \frac{1}{576f_\pi^4 \pi^2} \{ 77M_\pi^4 + M_\pi^2 (154M_\eta^2 - 72t) - 9[3(s^2 + su + u^2) + 8tM_\eta^2 - 9M_\eta^4] \} \\
& + \frac{1}{6f_\pi^4} \left\{ \frac{M_\pi^2}{9} \bar{J}_{\eta\eta}(t)(16M_K^2 - 7M_\pi^2) + \frac{t}{4} \bar{J}_{KK}(t)(9t - 2M_\pi^2 - 6M_\eta^2) + \bar{J}_{\pi\pi}(t)M_\pi^2 (2t - M_\pi^2) \right\} \\
& + \frac{1}{9f_\pi^4} \left\{ M_\pi^4 \bar{J}_{\pi\eta}(s) + \frac{1}{24} \bar{J}_{KK}(s) (9s - 8M_K^2 - M_\pi^2 - 3M_\eta^2)^2 + [s \leftrightarrow u] \right\}.
\end{aligned}$$

Finally, the KK scattering amplitudes were calculated in [11]. They were given in a rather different notation from the previous ones. Our result is, for $K^+K^- \rightarrow K^+K^-$:

$$\begin{aligned}
T_{ch}(s, t, u) &= \frac{2M_K^2 - u}{f_\pi^2} - \frac{\mu_K}{6f_\pi^2 M_K^2} [5(s^2 + st + t^2) + 6u^2 - 13uM_K^2 - 8M_K^4] \quad (B7) \\
& + \frac{\mu_\pi}{2f_\pi^2} \left\{ 5(u - 2M_K^2) - \frac{11s^2 + 8st + 11t^2 + 8uM_K^2 - 32M_K^4}{24M_\pi^2} + \frac{9(s^2 + t^2) + 24uM_K^2 - 64M_K^4}{16(M_K^2 - M_\pi^2)} \right\}
\end{aligned}$$

$$\begin{aligned}
& + \frac{\mu_\eta}{12f_\pi^2} \left\{ 64M_K^2 - 2M_\pi^2 - 27u - \frac{81(s^2 + t^2) - 36(s+t)M_\pi^2 + 8M_\pi^4}{12M_\eta^2} + \frac{9(s^2 + t^2) + 24uM_K^2 - 64M_K^4}{2(M_\pi^2 - M_\eta^2)} \right\} \\
& + \frac{4}{f_\pi^4} \left\{ 2L_2^r(u - 2M_K^2)^2 + (2L_1^r + L_2^r + L_3) [(s - 2M_K^2)^2 + (t - 2M_K^2)^2] - 4L_4^r u M_K^2 - 2L_5^r(u - 2M_K^2)M_\pi^2 \right. \\
& - 4[L_5^r - 2(2L_6^r + L_8^r)]M_K^4 \left. \right\} + \frac{186st - 177u^2 + 1032uM_K^2 - 1648M_K^4}{2304f_\pi^4\pi^2} + \frac{1}{2f_\pi^4}(u - 2M_K^2)^2 \bar{J}_{KK}(u) \\
& + \frac{1}{288f_\pi^4} \left\{ 60 [s(2s + t) + 4uM_K^2 - 8M_K^4] \bar{J}_{KK}(s) + 2(9s - 8M_K^2 - M_\pi^2 - 3M_\eta^2)^2 \frac{\bar{J}_{\pi\eta}(s)}{3} \right. \\
& \left. + (9s - 2M_\pi^2 - 6M_\eta^2)^2 \bar{J}_{\eta\eta}(s) + 3 [s(11s + 4t - 8M_K^2) - 8(s + 2t - 4M_K^2)M_\pi^2] \bar{J}_{\pi\pi}(s) + [s \leftrightarrow t] \right\}.
\end{aligned}$$

And for $\bar{K}^0 K^0 \rightarrow K^+ K^-$:

$$\begin{aligned}
T_{neu}(s, t, u) &= \frac{2M_K^2 - u}{2f_\pi^2} - \frac{\mu_K}{12f_\pi^2 M_K^2} \{ 5s^2 - su + 8u^2 - 2M_K^2(s + 16u) + 36M_K^4 \} \tag{B8} \\
& + \frac{\mu_\pi}{4f_\pi^2} \left\{ 5(u - 2M_K^2) - \frac{11s^2 + 4t^2 + 4s(2t + u) - 8(s + 2t)M_K^2}{12M_\pi^2} + \frac{24(s - 2t)M_K^2 - 9(s^2 - 2t^2) + 16M_K^4}{8(M_K^2 - M_\pi^2)} \right\} \\
& + \frac{\mu_\eta}{12f_\pi^2} \left\{ 9(s - u) + 14M_K^2 - M_\pi^2 - \frac{(9s - 2M_\pi^2)^2}{12M_\eta^2} + \frac{8M_K^2(3s - 6t + 2M_K^2) - 9(s^2 - 2t^2)}{2(M_\pi^2 - M_\eta^2)} \right\} \\
& + \frac{2}{f_\pi^4} \left\{ (4L_1^r + L_3)(s - 2M_K^2)^2 + 2L_2^r(u - 2M_K^2)^2 + (2L_2^r + L_3)(t - 2M_K^2)^2 \right\} \\
& + \frac{4}{f_\pi^4} \left\{ 4L_4^r s M_K^2 - 2M_K^4 [4L_4^r + L_5^r - 2(2L_6^r + L_8^r)] - L_5^r(u - 2M_K^2)M_\pi^2 \right\} \\
& - \frac{3(31s^2 + 4su + 16u^2) - 4M_K^2(30s + 57u - 80M_K^2)}{2304f_\pi^4\pi^2} \\
& + \frac{\bar{J}_{KK}(s)}{6f_\pi^4} [s(s - u) + 4M_K^2(2M_K^2 - t)] - \frac{\bar{J}_{\pi\eta}(s)}{432f_\pi^4} (9s - 8M_K^2 - M_\pi^2 - 3M_\eta^2)^2 + \frac{\bar{J}_{KK}(u)}{4f_\pi^4} (u - 2M_K^2)^2 \\
& + \frac{\bar{J}_{\pi\pi}(s)}{96f_\pi^4} [s(7s - 4t + 8M_K^2) + 8(s + 2t - 4M_K^2)M_\pi^2] + \frac{\bar{J}_{\pi\pi}(t)}{24f_\pi^4} (2s + t - 4M_K^2)(t - 4M_\pi^2) \\
& + \frac{\bar{J}_{\pi\eta}(t)}{216f_\pi^4} (9t - 8M_K^2 - M_\pi^2 - 3M_\eta^2)^2 + \frac{\bar{J}_{KK}(t)}{24f_\pi^4} [t(s + 2t) + 4uM_K^2 - 8M_K^4] + \frac{\bar{J}_{\eta\eta}(s)}{288f_\pi^4} (9s - 2M_\pi^2 - 6M_\eta^2)^2.
\end{aligned}$$

-
- [1] S. Weinberg, *Physica* A96, (1979) 327.
- [2] J. Gasser and H. Leutwyler, *Ann. Phys.* 158, (1984) 142.
- [3] J. Gasser and H. Leutwyler, *Nucl. Phys.* B250, (1985) 465,517,539.
- [4] H. Leutwyler “Chiral Dynamics”. Contribution to the Festschrift in honor of B.L. Ioffe. hep-ph/0008124. A. Dobado, A.Gómez-Nicola, A. L. Maroto and J. R. Peláez, *Effective Lagrangians for the Standard Model*, Texts and Monographs in Physics. ed: Springer-Verlag, Berlin-Heidelberg-New York (1997). A. Pich, *Rept.Prog.Phys.*58 (1995),563-610. U.G. Meißner, *Rept.Prog.Phys.*56 (1993),903-996.
- [5] V. Bernard, N. Kaiser and U.G. Meißner, *Nucl. Phys.* B364 (1991), 283. J.A. Oller, E. Oset, *Phys.Rev.*D60:074023,1999. M.Jamin, J.A. Oller, A.Pich, *Nucl.Phys.*B587 (2000), 331-362.
- [6] J.A. Oller, and E. Oset *Nucl. Phys.* A620 (1997), 438. J. Nieves, E. Ruiz Arriola. *Phys.Rev.*D63 (2001) 076001; *Phys. Lett.* B455 (1999) 30; *Nucl. Phys.* A679 (2000) 57.
- [7] T. N. Truong, *Phys. Rev. Lett.* 661, (1988) 2526 ;*Phys. Rev. Lett.* 67, (1991) 2260; A. Dobado, M.J.Herrero and T.N. Truong, *Phys. Lett.* B235, (1990) 134;
- [8] A. Dobado and J.R. Peláez, *Phys. Rev.* D47, (1993) 4883; *Phys. Rev.* D56, (1997) 3057.
- [9] J. A. Oller, E. Oset and J. R. Peláez, *Phys. Rev. Lett.* 80, (1998) 3452; *Phys. Rev.* D59, (1999) 074001; *Erratum-ibid.* D60, (1999) 099906.
- [10] V. Bernard, N. Kaiser, U.G. Meissner, *Phys. Rev.* D43 (1991), 2757; *Nucl. Phys.* B357 (1991), 129; *Phys. Rev.* D44 (1991), 3698.
- [11] F. Guerrero and J. A. Oller, *Nucl. Phys.* B537, (1999) 459. *Erratum-ibid.*B602, (2001), 641.
- [12] H. Leutwyler, *Phys. Lett.* B374, (1996) 163 and *Nucl. Phys.* B64 (Proc. Suppl), (1998) 223. R. Kaiser, diploma work, Bern University, 1997.
- [13] M. Gell-Mann, Caltech Report CTSL-20 (1961). S. Okubo, *Prog. Theor. Phys* 27 (1962) 949.
- [14] D. Iagolnitzer, J. Zinn-Justin and J.B. Zuber, *Nucl. Phys.* B60 233 (1973)
- [15] A. M. Badalyan, L. P. Kok, M.I. Polikarpov and Y.A. Simonov, *Phys. Rept.* 82, 31 (1982).
- [16] Z. Xiao and H. Zheng, hep-ph/0103042 and hep-ph/0107188.
- [17] M. Boglione, M.R. Pennington. *Z.Phys.*C75,113 (1997); I. P. Cavalcante, J. Sa Borges, hep-ph/0101037
- [18] A. Dobado, A. Gómez-Nicola and J.R.Peláez, in preparation.
- [19] S. D. Protopopescu *et al.*, *Phys. Rev.* D7, (1973) 1279.
- [20] P. Estabrooks and A.D.Martin, *Nucl.Phys.* B79, (1974) 301.
- [21] A. D. Martin and E. N. Ozmutlu, *Nucl. Phys.* B158, (1979) 520.
- [22] G.Grayner *et al.*, in *Experimental Meson Spectroscopy*, edited by A. H. Rosenfeld and K. W. Lai, AIP Conf. Proc. 8 (AIP, New York, 1972) p. 5; G.Grayner *et al.*, presented at the 16th Int. Conf. on High-Energy Physics, Batavia, 1972, paper No.768; B. Hyams *et al.**Nucl. Phys.* B64,134 (1973); W.Manner, presented at the 4th Int. Conf. on Experimental Meson Spectroscopy, Boston, MA, USA, April 1974,CERN preprint; G. Grayer *et al.*, *Nucl. Phys.* B75, (1974) 189.
- [23] P. Estabrooks *et al.*, in “ $\pi\pi$ Scattering”, edited by D.K. Williams and V.Hagopian, AIP Conf. Proc. 13 (AIP, New York,1973), p. 37.
- [24] C. D. Frogatt and J.L.Petersen, *Nucl. Phys.* B129, (1977) 89.
- [25] D. Cohen, *Phys. Rev.* D22, (1980) 2595.
- [26] A. Etkin *et al.* *Phys. Rev.* D25, 1786 (1982).
- [27] V. A. Polychronatos *et al.* *Phys. Rev.* D19,1317 (1979)
- [28] W. Wetzel *et al.*, *Nucl. Phys.* B115, 208 (1976)
- [29] S. J. Lindebaum and R.S. Longacre,*Phys. Lett.* B274, 492 (1992).
- [30] D. Morgan and M.R. Pennington, *Phys. Rev.* D48,1185 (1993).
- [31] W. Hoogland *et al.*, *Nucl. Phys.* B126, 109 (1977)
- [32] M. J. Losty *et al.*, *Nucl. Phys.* B69, 185 (1974).
- [33] L. Rosselet *et al.*, *Phys. Rev.* D15, (1977) 574.
- [34] P. Truöl for the E865 Collab., hep-ex/0012012, M. Zeller for the E865 Collab. “ $\pi\pi$ scattering from K_{14} decays” Talk presented in Chiral Dynamics 2000. (Available at: <http://www.jlab.org/intralab/calendar/chiral/>).
- [35] R. Mercer *et al.*, *Nucl. Phys.* B32, (1971) 381.
- [36] P. Estabrooks *et al.*, *Nucl. Phys.* B133, (1978) 490.
- [37] H. H. Bingham *et al.*, *Nucl. Phys.* B41, (1972) 1.
- [38] S. L. Baker *et al.*, *Nucl. Phys.* B99, (1975) 211.
- [39] D. Aston *et al.* *Nucl. Phys.* B296, (1988) 493.
- [40] D. Linglin *et al.*, *Nucl. Phys.* B57,64 (1973).
- [41] T.A. Armstrong *et al.*, *Z. Phys.* C52, 389-396 (1991)
- [42] G. Amorós, J. Bijnens and P. Talavera, *Nucl. Phys.* B585,293,(2000); *Erratum-ibid.*B598,665 (2001); *Nucl. Phys.* B602,87,(2001).
- [43] J. Bijnens, G. Colangelo and J. Gasser, *Nucl. Phys.* B427, (1994) 427.
- [44] J.R. Peláez, J.A. Oller and E. Oset, *Nucl. Phys.* A675 (2000) 92c.
- [45] The Particle Data Group, *Review of Particle Physics*, *Eur. Phys. J.* C15, 1-878 (2000).
- [46] E791 Collaboration,*Phys. Rev. Lett.* 86,(2001) 770. C. Gobel for the E791 Collab. hep-ex/0012009, and talk given in IX International Conference on Hadron Spectroscopy, HADRON2001, Protvino, Russia, August 2001 (to appear in the proceedings).
- [47] F. James, *Minuit Reference Manual* D506 (1994)
- [48] T.T. Wu and C. N. Yang, *Phys. Rev. Lett.* 13,380 (1964)
- [49] J. Gasser and U.-G. Meißner, *Phys. Lett.* B258 129 (1991).
- [50] R.L. Jaffe, *Phys. Rev.* D15 267 (1977); *Phys. Rev.* D15, 281 (1977). E. van Beveren *et al.* *Z. Phys.* C30, 615 (1986). S. Ishida *et al.*, *Prog. Theor. Phys.* 98,621 (1997).
- [51] D. Black, A. H. Fariborz, F. Sannino, J. Schechter. *Phys. Rev.* D58:054012,1998. M. Jamin, J.A.Oller, A. Pich *Nucl. Phys.* B587,331 (2000) E. van Beveren, G. Rupp, hep-ex/0106077.
- [52] S.N. Cherry, M.R. Pennington. *Nucl.Phys.* A688, 823 (2001).
- [53] S. M. Flatté, *Phys. Lett.* B63 224 (1976).
- [54] J.A. Oller, E. Oset and J. R. Peláez, *Phys. Rev.* D62, 114017 (2000).
- [55] O. Dumbrajs *et al* *Nucl. Phys.* B191 301 (1981).